

Emergent cavity-QED dynamics along the edge of a photonic lattice

Enrico Di Benedetto¹,^{*} Xuejian Sun,^{2,1,*} Marcel A. Pinto¹, Luca Leonforte¹, Chih-Ying Chang^{1,3,4}, Vincent Jouanny^{3,4}, Léo Peyruchat^{3,4}, Pasquale Scarlino^{1,3,4} and Francesco Ciccarello^{1,5}

¹Università degli Studi di Palermo, Dipartimento di Fisica e Chimica – Emilio Segrè, via Archirafi 36, I-90123 Palermo, Italy

²School of Physics and Telecommunication Engineering,
Zhoukou Normal University, 466001 Zhoukou, China

³Hybrid Quantum Circuits Laboratory (HQC), Institute of Physics,
École Polytechnique Fédérale de Lausanne (EPFL), 1015, Lausanne, Switzerland

⁴Center for Quantum Science and Engineering,
Institute of Physics, École Polytechnique Fédérale de Lausanne (EPFL), 1015, Lausanne, Switzerland

⁵NEST, Istituto Nanoscienze-CNR, Piazza S. Silvestro 12, 56127 Pisa (Italy)

(Dated: July 21, 2025)

We investigate qubits coupled to the boundary of a two-dimensional photonic lattice that supports *dispersionless* edge modes – unlike conventional edge modes that sustain propagating photons. As a case study, we consider a honeycomb lattice ("photonic graphene") of coupled resonators with a zigzag edge, where the edge modes form a flat band defined only over a restricted region of momentum space. We show that light-matter interactions are effectively captured by a dissipative cavity-QED model, wherein the emitter coherently couples to a fictitious cavity mode emerging as a superposition of edge modes. This mode has support on only one sublattice and, most notably, displays an unconventional power-law localization around the qubit – yet remaining normalizable in the thermodynamic limit – with a spatial range that can be tuned by introducing lattice anisotropy. We predict occurrence of vacuum Rabi oscillations and efficient state transfer between distant emitters. An experimental demonstration using superconducting circuits is proposed.

Two-dimensional (2D) photonic lattices with non-trivial topology support chiral edge modes that spectrally arise within bandgaps of bulk modes [1–3]. Coupling quantum emitters to an edge of such a photonic bath and adjusting their frequency within a bandgap thus enables tasks such as directional emission [4–8] and state transfer [9–11]. In such dynamics, an excited emitter typically undergoes an *irreversible* decay into the photonic edge modes, with these modes embodying a 1D continuum characterized by an associated dispersion relation.

Here, we predict that light-matter interactions on the edge of a 2D photonic lattice can exhibit a different character, resembling instead *reversible* cavity-QED dynamics although with a number of unconventional features. As a case study, we consider a set of qubits (two-level quantum emitters) coupled to the edge of photonic *graphene* [12], i.e., a semi-infinite 2D honeycomb lattice of coupled resonators. For suitable edge geometry, e.g., the *zigzag* boundary in Fig. 1(a), graphene can host topological edge modes, albeit of an unusual type [12–16] in that [cf. Fig. 1(b)]: (i) they are *dispersionless*, thus forming a 1D *flat band* [17] sustaining non-propagating photons; (ii) they exist only within a *limited* region of the first Brillouin zone (BZ), a major consequence being that they cannot be expanded in a basis of spatially compact modes [18] unlike usual flat bands

[19]; (iii) spectrally they do not lie within a bandgap but rather touch both the bands of bulk modes at the Dirac points [see Fig. 1(b)]. Our goal here is investigating light-matter interactions when qubits are tuned near the frequency of edge modes of this kind.

Since these modes are frequency-degenerate, one might expect an emitter to effectively couple to a specific superposition of the edge modes that is spatially-localized around its position [20, 21]. This picture, reducing the dynamics to an effective Jaynes-Cummings model [22, 23] with the localized mode playing the role

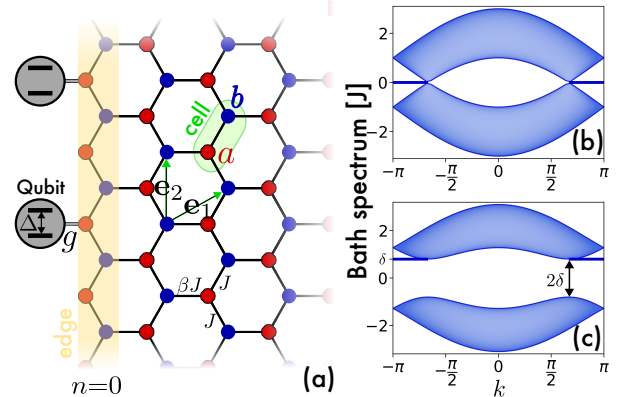


Figure 1. (a) Qubits (two-level emitters) coupled to a zigzag edge of a 2D honeycomb lattice of coupled resonators (*photonic graphene*). The bare frequency of a/b resonators is $\pm\delta$ (not shown). (b)-(c) Spectrum of bath normal modes in the gapless case $\delta=0$ (b) and gapped case $\delta>0$ (c). In (b) and (c), a set of dispersionless edge modes (partial flat band) arises at frequency zero and δ , respectively.

* Correspondence email address: Xuejian890@gmail.com

of the cavity, indeed typically applies to conventional photonic flat bands spanning the whole BZ and spectrally gapped from other bands [20, 21]. In those cases, the fictitious cavity mode is usually exponentially localized around the emitter with the mode's localization length representing an effective cavity volume. In the present lattice, however, edge modes are not gapped from bands of bulk modes and, moreover, their support does not span the full BZ [see Fig. 1(b)], which plays against existence an exponentially-localized superposition. This raises the question of whether a cavity-QED-like model can be defined to capture the physics of the present system.

We will find that an effective localized-mode picture is still possible, but in a broader – and, in some respects, unconventional – sense. In particular, the emergent localized mode shows an atypical power-law decay in real space away from the qubit. Building on this, we present an effective cavity-QED effective model for many qubits, accounting for losses into bulk lattice modes, which is used to predict occurrence of vacuum Rabi oscillations and state transfer between emitters.

Model.— Our photonic bath B is a 2D honeycomb lattice of coupled single-mode resonators [see Fig. 1(a)] whose Hamiltonian reads (throughout we set $\hbar = 1$)

$$H_B = \delta \sum_{\mathbf{R}} (a_{\mathbf{R}}^\dagger a_{\mathbf{R}} - b_{\mathbf{R}}^\dagger b_{\mathbf{R}}) + \sum_{\langle \mathbf{R}, \mathbf{R}' \rangle} J_{\langle \mathbf{R}, \mathbf{R}' \rangle} (a_{\mathbf{R}}^\dagger b_{\mathbf{R}'} + \text{H.c.}), \quad (1)$$

where $\mathbf{R} = n\mathbf{e}_1 + m\mathbf{e}_2$ specifies the unit cell position (with $\mathbf{e}_{1(2)}$ primitive vectors and n, m integers), while $a_{\mathbf{R}} \equiv a_{nm}$ and $b_{\mathbf{R}} \equiv b_{nm}$ are standard bosonic ladder operators (here $\langle \mathbf{R}, \mathbf{R}' \rangle$ denotes nearest-neighbor resonators). In Eq. (1), $\pm\delta$ is the bare frequency of a - and b -resonators, while $J_{\langle \mathbf{R}, \mathbf{R}' \rangle}$ is the photon hopping rate [see Fig. 1(a)]. Unless otherwise stated, we will set $J_{\langle \mathbf{R}, \mathbf{R}' \rangle} = J$ [corresponding to $\beta=1$ in Fig. 1(a)]. For $\delta=0$, Eq. (1) is the bosonic analogue of the celebrated tight-binding Hamiltonian of graphene [12]. Importantly, as shown in Fig. 1(a), here we consider a *semi-infinite* lattice with a zigzag edge (resonators $a_{n=0m}$ and $b_{n=0m}$). Accordingly, $n = 0, 1, 2, \dots$ while $m \in \mathbb{Z}$.

A set of qubits (two-level emitters), each with ground (excited) state $|g_j\rangle$ ($|e_j\rangle$) whose energy separation is Δ , are locally weakly-coupled under the rotating-wave approximation to a -resonators [see Fig. 1(a)]. The total Hamiltonian thus reads

$$H = \Delta \sum_j \sigma_j^\dagger \sigma_j + H_B + g \sum_j \left(a_{\mathbf{R}_j}^\dagger \sigma_j + \text{H.c.} \right), \quad (2)$$

with $\sigma_j = |g_j\rangle\langle e_j|$ the pseudo-spin ladder operator of the j th qubit, g the atom-photon coupling strength and where $\mathbf{R}_j \equiv (0, m_j)$ labels the edge resonator which qubit j is coupled to.

Bulk and edge modes of H_B .— By enforcing periodic boundary conditions *along* the edge direction \mathbf{e}_2

[cf. Fig. 1(a)], whose corresponding momentum component is called k , the bath Hamiltonian (1) can be exactly mapped to a set of uncoupled 1D Rice-Mele models [24], each labeled by k and having an edge at $n=0$ (see e.g. Ref. [15]). This allows to express H_B in the diagonal form [25]

$$H_B = \sum_{\mu=\pm} \int_0^\pi dq \int_{-\pi}^\pi dk \omega_\mu(k, q) \mathcal{B}_\mu^\dagger(k, q) \mathcal{B}_\mu(k, q) + \delta \int_{2\pi/3 < |k| \leq \pi} dk \mathcal{E}_k^\dagger \mathcal{E}_k \quad (3)$$

with q the momentum component corresponding to direction \mathbf{e}_1 (from edge to bulk). Two symmetric bands of bulk modes $\mathcal{B}_\pm(k, q)$ arise. For $\delta=0$, their spectra $\omega_\pm(k, q)$ [see Fig. 1(b)-(c)] are the same as those for bulk graphene [12]. These bands touch at the Dirac points ($q=\pi$, $k=\pm 2\pi/3$), while for $\delta>0$ a gap of width 2δ opens up. Besides the bands of bulk modes, the lattice additionally hosts a set of *dispersionless edge modes* \mathcal{E}_k with common frequency δ , where, importantly, k takes only values external to the two Dirac points. Modes \mathcal{E}_k thus form a *partial* flat band [cf. Fig. 1(b)-(c)]. Their real-space representation is $\mathcal{E}_k = \sum_{n,m} \varepsilon_k(n, m) a_{nm}$, where

$$\varepsilon_k(n, m) = \frac{\mathcal{N}_k}{\sqrt{2\pi}} (-1)^n e^{-ik(m+n/2)} e^{-n/\lambda_k}, \quad (4)$$

with $\mathcal{N}_k = \sqrt{-(1+2\cos k)}$ and $\lambda_k^{-1} = \ln |J/\mathcal{J}_k|$ for $\mathcal{J}_k = 2J \cos(k/2)$. Edge modes \mathcal{E}_k thus have support only on the a -sublattice, being localized on the edge $n=0$ with a penetration length λ_k ranging between 0 (for $k=\pm\pi$) and infinity (for $k=\pm 2\pi/3$). Their emergence for $\delta=0$ can indeed be linked [26] to well-known zero-energy edge states of the standard SSH model in the non-trivial phase protected by sublattice, i.e., chiral, symmetry [24]. For $\delta>0$ (open gap), chiral symmetry is lost, but edge modes are unaffected with their frequency now shifted by δ [26].

Effective cavity-QED model for $\delta=0$: one qubit.— We first set $\delta=0$ [cf. Fig. 1(b)] and consider only one qubit [thus we drop subscript j in (2)] coupled to the resonator a_{00} . We expand a_{00} in terms of modes \mathcal{E}_k (having zero frequency) and $\mathcal{B}_\pm(k, q)$ so as to split the coupling Hamiltonian [last term in Eq. (2)] into one contribution from edge modes and one from bulk modes. The former can be recast as $g(\mathcal{C}^\dagger \sigma + \text{H.c.})$ with $\mathcal{C} = \sum_k \varepsilon_k^*(0, 0) \mathcal{E}_k$ a superposition mode which is itself a zero-frequency normal mode of H_B whose detuning from the qubit is measured by Δ . For g and $|\Delta|$ small enough compared to J , this contribution will dominate over the one from bulk modes, whose density of states vanishes on approaching the Dirac points [27], which can be treated as a Markovian bath [28]. We thus end up with a master equation for the joint density matrix ρ of the qubit and mode \mathcal{C} [25], reading

$$\dot{\rho} = -i \left[\Delta \sigma^\dagger \sigma + \Omega (\mathcal{C}^\dagger \sigma + \text{H.c.}), \rho \right] + \gamma(\Delta) \mathcal{D}_\sigma[\rho], \quad (5)$$

where $\mathcal{D}_O[\rho] = O\rho O^\dagger - \{O^\dagger O, \rho\}/2$ is the usual Lindblad dissipator, $\Omega = g/\sqrt{\mathcal{A}}$ with $\mathcal{A}^{-1} = \sqrt{3}/\pi - 1/3$ is the qubit-mode interaction strength (proportional to the vacuum Rabi frequency on resonance) and $\gamma(\Delta)$ is the Δ -dependent decay rate into bulk modes (we incorporated factor $\sqrt{\mathcal{A}}$ in the definition of \mathcal{C}). For $|\Delta| \ll J$, we can approximate $\gamma(\Delta) \simeq 4g^2 |\Delta|/(\sqrt{3}J^2)$ [25], which vanishes for $\Delta \rightarrow 0$. Eq. (5) defines an effective dissipative Jaynes-Cummings model [29] where a lossy qubit coherently couples to a fictitious *cavity* embodied by the superposition mode \mathcal{C} . We point out that the validity of (5) relies crucially on whether mode \mathcal{C} is normalized so as to ensure $[\mathcal{C}, \mathcal{C}^\dagger] = 1$. Indeed, in real space it reads $\mathcal{C} = \sqrt{\mathcal{A}} \sum_{nm} c(n, m) a_{nm}$ with [cf. Eq. (4)]

$$c(n, m) = \int_{\frac{2\pi}{3} < |k| < \pi} dk \varepsilon_k^*(0, 0) \varepsilon_k(n, m). \quad (6)$$

In the thermodynamic limit, one can show that $\sum_{n,m} |c(n, m)|^2 = \mathcal{A}^{-1}$, hence mode \mathcal{C} is normalized. Accordingly, \mathcal{A} is naturally interpreted as a (2D) *cavity volume* yielding a finite Rabi frequency. This emergent cavity mode however has a non-standard (to our knowledge unprecedented) shape, whose spatial distribution is plotted in Fig. 2(a) using Eq. (6). The mode has support on the *a*-sublattice only, which is inherited from edge modes \mathcal{E}_k . More remarkably, along the edge direction (resonators $a_{n=0m}$), the integral in (6) can be evaluated exactly and yields $c(0, 0) = \mathcal{A}^{-1}$, $c(0, \pm 1) = \sqrt{3}/(4\pi) - 1/3$ while for $|m| \geq 2$

$$c(0, m) = \frac{2}{3} \left[s(|m| - 1) + s(|m|) + s(|m| + 1) \right] \quad (7)$$

where $s(x) = \sin(2\pi x/3)/(2\pi x/3)$. Fig. 2(b) (blue curve) shows a plot of $c(0, m)$ versus m , which is easily checked to scale as $\sim |m|^{-2}$ for large $|m|$. Towards the bulk, on the other hand, the mode localization is stronger but still power law since $c(n \gg 1, m) \sim |n|^{-2}$ [25]. Thus, the mode shows up an anomalous power-law localization around the qubit with nodes on *b*-resonators. Still \mathcal{C} is normalizable, yielding finite cavity volume \mathcal{A} and Rabi frequency Ω .

Based on (5), the dynamics of an initially-excited qubit generally undergoes damped vacuum Rabi oscillations with oscillation frequency $\Omega_R(\Delta) = \sqrt{\Delta^2 + 4\Omega^2}$ and damping rate $\gamma(\Delta)$. For small Δ/J , the coherent coupling to mode \mathcal{C} dominates over dissipation into bulk modes, whereas the opposite holds for Δ large enough. This is displayed in Fig. 2(c) for $g = 0.05J$ and different values of Δ/J , showing that the solution predicted through (5) matches the exact numerical simulations based on the full Hamiltonian (2).

Cavity-QED model for $\delta=0$: many qubits.— We next generalize to many qubits [cf. Eq. (2)]. Under conditions analogous to those underpinning (5) plus the standard

assumption that emitters are not too distant so as to make retardation effects negligible [30], the bulk modes can be treated as a common Markovian bath for the qubits. The interaction of qubit j to modes \mathcal{E}_k 's can again be arranged as the coupling to an effective cavity mode $\tilde{\mathcal{C}}_j$ defined analogously to \mathcal{C} [cf. Eq. (6)] but the replacement $c(n, m) \rightarrow c(n, m - m_j)$. Zero-frequency modes $\{\tilde{\mathcal{C}}_j\}$, which are as many as the number of qubits N_q , are however spatially overlapping and non-orthogonal. Still, similarly to Ref. [20], they can be orthonormalized yielding the new set of modes $\mathcal{C}_j = \sum_{j'} (\mathbf{M}^{-1})_{jj'} \tilde{\mathcal{C}}_{j'}$ with the $N_q \times N_q$ invertible matrix \mathbf{M} such that $\mathbf{M}\mathbf{M}^\dagger = \mathbf{P}$, where $P_{ij} = c(0, m_j - m_i)$. The resulting modes fulfill $[\mathcal{C}_i, \mathcal{C}_j^\dagger] = \delta_{ij}$ and thus can be viewed as independent cavity modes (one for each qubit). Note that, although orthogonal, these are still spatially overlapping, hence each emitter i is generally coupled to all modes \mathcal{C}_j 's (not only to \mathcal{C}_i). Based on the above, a generalization of the procedure leading to Eq. (5) returns the collective master equation

$$\dot{\rho} = -i \left[\Delta \sum_j \sigma_j^\dagger \sigma_j + g \sum_{ij} (\mathcal{C}_i^\dagger M_{ij} \sigma_j + \text{H.c.}), \rho \right] + \mathcal{L}[\rho], \quad (8)$$

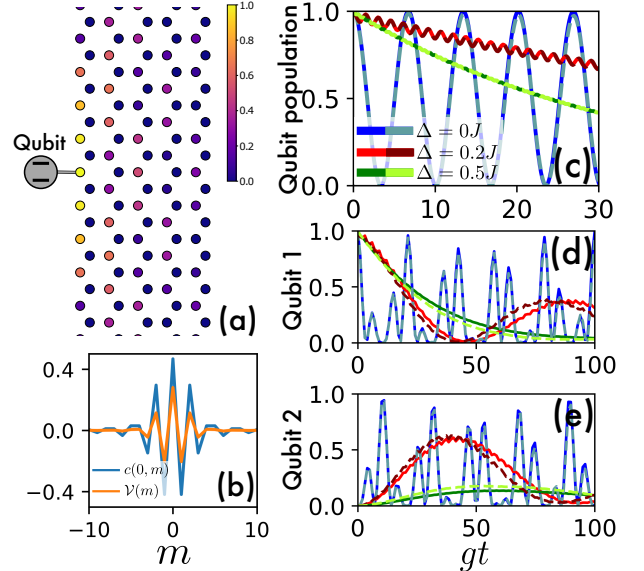


Figure 2. (a) Real-space distribution (modulus) of mode \mathcal{C} for one qubit coupled to $a_{0,0}$ (we used a logarithmic color scale and rescaled to the maximum value). (b) Mode amplitude $c(0, m)$ along the edge (blue) [cf. Eq. (6)]. We also plot (orange curve) the qubit-qubit interaction potential $\mathcal{V}(m)$ [cf. Eq. (9)] for $\delta=0.3J$ and $\Delta=0.05J$. (c) Excited-state population versus time for an initially excited qubit coupled to a_{00} for different values of Δ/J . (d)-(e) Excitation transfer between two emitters, one coupled to resonator a_{00} (qubit 1) one to a_{02} (qubit 2), for the initial state $|e_{1g2}\rangle$ and the same values of Δ as in (c). In (c)-(e), where we set $g = 0.05J$, solid and dashed lines are respectively the analytical solutions using (5) and numerical solutions based of the full model (2) for 600×600 units cells. The color legend in (d)-(e) is the same as in (c).

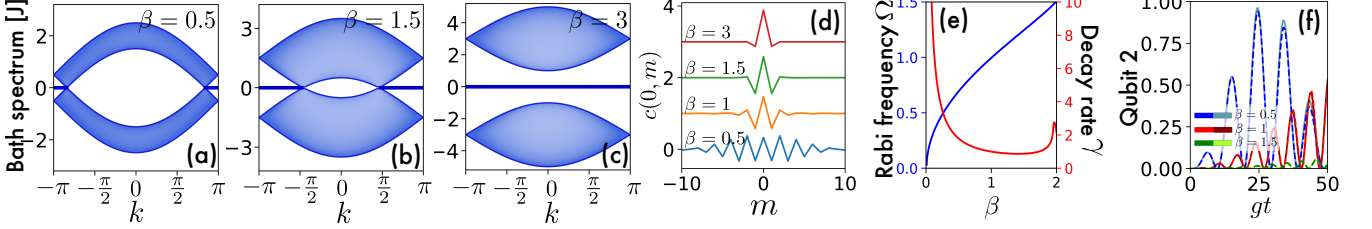


Figure 3. (a)-(d) Bath spectrum [(a)-(c)] and amplitude $c(0, m)$ (d) for different values of the anisotropy parameter β . In (d), for clarity curves for $\beta = 1, 1.5, 3$ are shifted upward by 1, 2, 3, respectively. (e) Rabi frequency Ω (blue) and loss rate γ (red) versus β for $\Delta=0.05J$ (rescaled to their $\beta=1$ values). (f) Qubit 2 population for two emitters at distance $m_1 - m_2 = 6$ with qubit 1 (2) initially excited (unexcited) for $\beta = 0.5, 1, 1.5$ and $\Delta=0$. In (f), we set $g=0.05J$.

where $\mathcal{L}[\rho] = \sum_{ij} \gamma_{ij}(\Delta) [\sigma_j \rho \sigma_i - \{\sigma_i^\dagger \sigma_j, \rho\}/2]$ is a many-qubit dissipator depending on rates γ_{ij} . For Δ small enough, these can be approximated as $\gamma_{ij}(\Delta) \simeq 4g^2 |\Delta| \cos(2\pi|m_i - m_j|/3) / (\sqrt{3}J^2)$ (vanishing for $\Delta \rightarrow 0$). Fig. 2(d)-(e) shows the population dynamics of two qubits coupled to resonators a_{00} and a_{02} with the former (latter) initially excited (unexcited). A generally incomplete (due to losses into bulk modes) excitation transfer occurs for $|\Delta| > 0$. For $\Delta=0$ (resonant coupling to edge modes), however, state transfer is achieved with fidelity 0.93 [see Fig. 2(d-e)]. The characteristic beatings, absent in the one-qubit dynamics of Fig. 2(c), are a signature that *two* effective modes (\mathcal{C}_1 and \mathcal{C}_2) participate to the dynamics.

Dispersive dipole-dipole interactions for $\delta > 0$.—In general, photon-mediated qubit-qubit interactions can be made dissipationless, entailing perfect state transfer, in the dispersive regime [31–38]. The cavity-QED model (8), however, does not admit a dispersive regime [39] since this would in particular require to detune emitters from \mathcal{C} by increasing $|\Delta|$, which however comes at the cost of enhanced dissipation into bulk modes (as $\gamma_{ij} \propto |\Delta|$). This regime is instead possible for $\delta > 0$ [cf. Eq. (2) and Fig. 1(c)], which opens a gap in the bath spectrum while spectrally shifting modes \mathcal{E}_k 's by δ . By tuning the qubits within the gap in a way that $|\Delta| < \delta$, their dynamics becomes dissipationless being described by the effective Hamiltonian $\mathcal{H}_{\text{eff}} = \sum_{ij} \mathcal{K}_{ij} \sigma_i^\dagger \sigma_j$ with $\mathcal{K}_{ij} = \frac{g^2}{\Delta - \delta} \mathcal{V}(m_i - m_j)$, where we defined

$$\mathcal{V}(m) = c(0, m) + (\Delta - \delta) G_{\text{bulk}}(m). \quad (9)$$

Here, $G_{\text{bulk}}(m)$ is the matrix element of the bulk modes resolvent at frequency Δ between sites \mathbf{R}_i and \mathbf{R}_j , which depends only on distance $m = m_i - m_j$ [25]. The dipole-dipole interaction potential (9) thus comprises a term due to edge modes, having exactly the same shape as mode \mathcal{C} [cf. Eq. (7) and Fig. 2(b)] plus a contribution due to the dispersive coupling to bulk modes. The shape of $\mathcal{V}(m)$, plotted in Fig. 2(b), is very similar to $c(0, m)$ exhibiting an analogous power-law scaling $\sim |m|^{-2}$.

Anisotropic lattice.— Much of the above physics stems from the property that modes \mathcal{E}_k have support only on the *limited* region of the BZ external to the pair of Dirac

points [cf. Fig. 1(b)-(c)]. The size of this region can be changed by making the honeycomb lattice *anisotropic*, allowing us to study the impact of anisotropy on the previous cavity-QED picture. We thus relax the constraint $J_{\langle \mathbf{R}, \mathbf{R}' \rangle} = J$ [cf. Eq. (2)] and set now to βJ the hopping rate between resonators $b_{\mathbf{R}}$ and $a_{\mathbf{R}+\mathbf{e}_1}$ [see bottom of Fig. 1(a)] with $\beta > 0$ an anisotropy parameter; hence the previous system retrieved for $\beta=1$. For the sake of argument, we set $\delta=0$.

Two bands of bulk modes and a set of zero-frequency edge modes \mathcal{E}_k still occur [see Fig. 3(a)-(c)] [40]. For $\beta < 2$, the modes \mathcal{E}_k still arise outside the two Dirac points, which however now lie at $k = \pm 2 \arccos(\beta/2)$. As β decreases below 1, the support of the partial flat band progressively shrinks, whereas it broadens as β increases above 1 until matching the full BZ for $\beta=2$. As long as $\beta < 2$, one can still define a cavity-QED model as in Eq. (5) with the superposition mode \mathcal{C} , Ω and γ now β -dependent. Along the edge direction, the amplitude of \mathcal{C} can be still analytically computed as ($|m| \geq 2$)

$$c(0, m) \propto s_\beta(|m| - 1) + (2 - \beta^2) s_\beta(|m|) + s_\beta(|m| + 1) \quad (10)$$

with $s_\beta(x) = \sin(tx)/(tx)$ for $t = 2 \arccos(\beta/2)$. Compared to Eq. (7), this still scales as $\sim |m|^{-2}$ but, remarkably, has larger width as β is reduced below 1, as shown in Fig. 3(d). Correspondingly, as shown in Fig. 3(e), the Rabi frequency $\Omega \propto \mathcal{A}^{-1/2}$ decreases, while the single-qubit loss rate, approximated as $\gamma \simeq 4|\Delta|/(J^2 \beta \sqrt{4 - \beta^2})$, becomes stronger. The broadening of \mathcal{C} substantially impacts excitation transfer in the case of many qubits. An instance is reported in Fig. 3(f), where state transfer between two qubits separated by six unit cells is achieved with fidelity $\simeq 0.94$ for $\beta=0.5$ in a time $g\tau \simeq 25$. In contrast, at time τ the transfer process is still in the early stages for $\beta=1$ and negligible for $\beta=1.5$.

For $\beta > 2$, Dirac points no longer exist with the edge modes now forming a flat band gapped from bulk modes and extended across the full BZ, which results in finite-ranged cavity-QED dynamics. Nonetheless, even in this case compact states cannot be defined unlike standard FBs [21].

Experimental implementation.— A proof-of-principle experimental demonstration of these phenomena is

within reach in circuit-QED platforms using transmon qubits emitting into a lattice of capacitively-coupled LC resonators [35, 41–43]. Suitable resonator geometries [44] allow for a straightforward realization of a honeycomb lattice of at least $\sim 30 \times 30$ resonators with a zigzag termination. Typical parameters are $J/2\pi = 100$ – 200 MHz, $g/2\pi \sim 20$ MHz and a resonator frequency $\omega_r/2\pi \sim 6$ GHz. The typical relative disorder on ω_r is $\sim 0.2\%$, while the next-nearest-neighbor hopping rate is $\sim 5\%$ [25, 41, 44]. With $g/2\pi = 20$ MHz, the resulting dynamics occurs on a ~ 330 ns timescale, well within the coherence times of transmon qubits ($\gtrsim 5 \mu\text{s}$) [35, 43].

Conclusions.— We studied a system of qubits emitting into the boundary of a 2D lattice sustaining dispersionless edge modes defined on a limited region of the BZ (partial flat band). The essential physics is captured by an effective cavity-QED model, where the emitter leaks into bulk modes and at the same couples to an emergent mode showing an unusual power-law localization. The range of this mode, which is connected to the length of the flat band support in the BZ, affects substantially photon-mediated qubit-qubit interactions, benefiting in particular long-range state transfer.

We note that, rigorously speaking, for $\delta=0$ and $\beta < 2$ the Markovian model (5) is valid for $\Delta \neq 0$ since the bath resolvent is singular at the Dirac points. Such singularity is very similar to the one occurring for qubits coupled to the *bulk* of a honeycomb lattice, which was shown to lead to non-Markovian decay [45, 46]. In our system, as long as the coupling strength is weak as in all previous instances, such non-Markovian effects are

negligible for all practical purposes or manifest at extremely long times, which is supported by the excellent agreement between the cavity-QED model and exact numerical simulations.

We point out that coupling qubits to *bulk* resonators is experimentally demanding with current circuit-QED technology, which provides a further major motivation/advantage for the present study.

From the perspective of topological photonics [2], our work introduces a new paradigm of light-matter interactions when emitters are coupled to edge modes of a 2D lattice. On the other hand, it unveils a novel system yielding power-law photon-mediated interactions, which are known to lead to a number of phenomena such as exotic many-body phases [47–51].









Acknowledgements.— XS acknowledges financial support from China Scholarship Council (Grant No. 202208410355). We acknowledge financial support from European Union-Next Generation EU through projects: PRIN 2022–PNRR No. P202253RLY “Harnessing topological phases for quantum technologies”; THENCE–Partenariato Esteso NQSTI–PE00000023–Spoke 2 “Taming and harnessing decoherence in complex networks”. P.S. acknowledges support from the Swiss State Secretariat for Education, Research and Innovation (SERI) under contract numbers UeM019-16 and MB22.00081 / REF-1131-52105. P.S. also acknowledges support from the Swiss National Science Foundation (SNSF), Grant number 200021_200418 / 1.

-
- [1] M. Kim, Z. Jacob, and J. Rho, Recent advances in 2d, 3d and higher-order topological photonics, *Light: Science & Applications* **9**, 130 (2020).
 - [2] T. Ozawa, H. M. Price, A. Amo, N. Goldman, M. Hafezi, L. Lu, M. C. Rechtsman, D. Schuster, J. Simon, O. Zeitler, and I. Carusotto, Topological photonics, *Rev. Mod. Phys.* **91**, 015006 (2019).
 - [3] B. Weber, M. S. Fuhrer, X.-L. Sheng, S. A. Yang, R. Thomale, S. Shamim, L. W. Molenkamp, D. Cobden, D. Pesin, H. J. Zandvliet, *et al.*, 2024 roadmap on 2d topological insulators, *Journal of Physics: Materials* **7**, 022501 (2024).
 - [4] S. Barik, A. Karasahin, C. Flower, T. Cai, H. Miyake, W. DeGottardi, M. Hafezi, and E. Waks, A topological quantum optics interface, *Science* **359**, 666 (2018).
 - [5] M. Jalali Mehrabad, A. P. Foster, R. Dost, E. Clarke, P. K. Patil, A. M. Fox, M. S. Skolnick, and L. R. Wilson, Chiral topological photonics with an embedded quantum emitter, *Optica* **7**, 1690 (2020).
 - [6] J. C. Owens, M. G. Panetta, B. Saxberg, G. Roberts, S. Chakram, R. Ma, A. Vrajitoarea, J. Simon, and D. I. Schuster, Chiral cavity quantum electrodynamics, *Nature Physics* **18**, 1048 (2022).
 - [7] C. Vega, D. Porras, and A. González-Tudela, Topological multimode waveguide qed, *Phys. Rev. Res.* **5**, 023031 (2023).
 - [8] D. Suárez-Forero, M. Jalali Mehrabad, C. Vega, A. González-Tudela, and M. Hafezi, Chiral quantum optics: recent developments and future directions, *Prx Quantum* **6**, 020101 (2025).
 - [9] N. Y. Yao, C. R. Laumann, A. V. Gorshkov, H. Weimer, L. Jiang, J. I. Cirac, P. Zoller, and M. D. Lukin, Topologically protected quantum state transfer in a chiral spin liquid, *Nature communications* **4**, 1585 (2013).
 - [10] M.-A. Lemonde, V. Peano, P. Rabl, and D. G. Angelakis, Quantum state transfer via acoustic edge states in a 2d optomechanical array, *New Journal of Physics* **21**, 113030 (2019).
 - [11] C. Dłaska, B. Vermersch, and P. Zoller, Robust quantum state transfer via topologically protected edge channels in dipolar arrays, *Quantum Science and Technology* **2**, 015001 (2017).
 - [12] A. H. Castro Neto, F. Guinea, N. M. R. Peres, K. S. Novoselov, and A. K. Geim, The electronic properties of graphene, *Rev. Mod. Phys.* **81**, 109 (2009).
 - [13] M. Fujita, K. Wakabayashi, K. Nakada, and K. Kusakabe,

- Peculiar localized state at zigzag graphite edge, *Journal of the Physical Society of Japan* **65**, 1920 (1996).
- [14] K. Nakada, M. Fujita, G. Dresselhaus, and M. S. Dresselhaus, Edge state in graphene ribbons: Nanometer size effect and edge shape dependence, *Physical Review B* **54**, 17954 (1996).
- [15] T. Tan, C. Li, and W. Yao, Edge state in ab-stacked bilayer graphene and its correspondence with the su-schrieffer-heeger ladder, *Phys. Rev. B* **104**, 245419 (2021).
- [16] M. Kohmoto and Y. Hasegawa, Zero modes and edge states of the honeycomb lattice, *Phys. Rev. B* **76**, 205402 (2007).
- [17] D. Leykam, A. Andreanov, and S. Flach, Artificial flat band systems: from lattice models to experiments, *Advances in Physics: X* **3**, 1473052 (2018).
- [18] J.-H. Park and J.-W. Rhim, Quasi-localization and wannier obstruction in partially flat bands, *Communications Physics* **7**, 179 (2024).
- [19] J.-W. Rhim and B.-J. Yang, Classification of flat bands according to the band-crossing singularity of Bloch wave functions, *Phys. Rev. B* **99**, 045107 (2019).
- [20] D. De Bernardis, Z.-P. Ciani, I. Carusotto, M. Hafezi, and P. Rabl, Light-Matter Interactions in Synthetic Magnetic Fields: Landau-Photon Polaritons, *Phys. Rev. Lett.* **126**, 103603 (2021).
- [21] E. Di Benedetto, A. González-Tudela, and F. Ciccarello, Dipole-dipole interactions mediated by a photonic flat band, *Quantum* **9**, 1671 (2025).
- [22] E. Jaynes and F. Cummings, Comparison of quantum and semiclassical radiation theories with application to the beam maser, *Proceedings of the IEEE* **51**, 89 (1963).
- [23] S. Haroche and J.-M. Raimond, *Exploring the quantum: atoms, cavities, and photons* (Oxford university press, 2006).
- [24] J. K. Asbóth, L. Oroszlány, and A. Pályi, *A short course on topological insulators*, Vol. 919 (Springer, 2016).
- [25] See Supplemental Material at [url] for further details.
- [26] S. Ryu and Y. Hatsugai, Topological origin of zero-energy edge states in particle-hole symmetric systems, *Physical review letters* **89**, 077002 (2002).
- [27] S. M. Girvin and K. Yang, *Modern Condensed Matter Physics* (Cambridge University Press, 2019).
- [28] H.-P. Breuer and F. Petruccione, *The theory of open quantum systems* (OUP Oxford, 2002).
- [29] S. Lorenzo, F. Lombardo, F. Ciccarello, and G. M. Palma, Quantum non-Markovianity induced by Anderson localization, *Sci Rep* **7**, 42729 (2017).
- [30] B. Windt, M. Bello, D. Malz, and J. I. Cirac, Effects of retardation on many-body superradiance in chiral waveguide qed, *Phys. Rev. Lett.* **134**, 173601 (2025).
- [31] J. S. Douglas, H. Habibian, C.-L. Hung, A. V. Gorshkov, H. J. Kimble, and D. E. Chang, Quantum many-body models with cold atoms coupled to photonic crystals, *Nature Photon* **9**, 326 (2015).
- [32] A. González-Tudela, C.-L. Hung, D. E. Chang, J. I. Cirac, and H. J. Kimble, Subwavelength vacuum lattices and atom-atom interactions in two-dimensional photonic crystals, *Nature Photon* **9**, 320 (2015).
- [33] M. Bello, G. Platero, J. I. Cirac, and A. González-Tudela, Unconventional quantum optics in topological waveguide qed, *Science Advances* **5**, eaaw0297 (2019).
- [34] N. M. Sundaresan, R. Lundgren, G. Zhu, A. V. Gorshkov, and A. A. Houck, Interacting Qubit-Photon Bound States with Superconducting Circuits, *Physical Review X* **9**, 011021 (2019).
- [35] M. Scigliuzzo, G. Calajò, F. Ciccarello, D. Perez Lozano, A. Bengtsson, P. Scarlino, A. Wallraff, D. Chang, P. Delsing, and S. Gasparinetti, Controlling Atom-Photon Bound States in an Array of Josephson-Junction Resonators, *Phys. Rev. X* **12**, 031036 (2022).
- [36] X. Zhang, E. Kim, D. K. Mark, S. Choi, and O. Painter, A superconducting quantum simulator based on a photonic-bandgap metamaterial, *Science* **379**, 278 (2023).
- [37] L. Leonforte, X. Sun, D. Valenti, B. Spagnolo, F. Illuminati, A. Carollo, and F. Ciccarello, Quantum optics with giant atoms in a structured photonic bath, *Quantum Science and Technology* **10**, 015057 (2024).
- [38] L. Leonforte, A. Carollo, and F. Ciccarello, Vacancy-like dressed states in topological waveguide qed, *Phys. Rev. Lett.* **126**, 063601 (2021).
- [39] H. Ritsch, P. Domokos, F. Brennecke, and T. Esslinger, Cold atoms in cavity-generated dynamical optical potentials, *Rev. Mod. Phys.* **85**, 553 (2013).
- [40] M. Kohmoto and Y. Hasegawa, Zero modes and edge states of the honeycomb lattice, *Physical Review B—Condensed Matter and Materials Physics* **76**, 205402 (2007).
- [41] D. Underwood, W. Shanks, A. C. Li, L. Ateshian, J. Koch, and A. A. Houck, Imaging photon lattice states by scanning defect microscopy, *Physical Review X* **6**, 021044 (2016).
- [42] A. Morvan, M. Féchant, G. Aiello, J. Gabelli, and J. Estève, Observation of topological valley hall edge states in honeycomb lattices of superconducting microwave resonators, *Optical Materials Express* **11**, 1224 (2021).
- [43] E. Kim, X. Zhang, V. S. Ferreira, J. Banker, J. K. Iverson, A. Sipahigil, M. Bello, A. González-Tudela, M. Mirhosseini, and O. Painter, Quantum electrodynamics in a topological waveguide, *Physical Review X* **11**, 011015 (2021).
- [44] V. Jouanny, S. Frasca, V. J. Weibel, L. Peyruchat, M. Scigliuzzo, F. Oppliger, F. De Palma, D. Sbroggiò, G. Beaulieu, O. Zilberberg, *et al.*, High kinetic inductance cavity arrays for compact band engineering and topology-based disorder meters, *Nature Communications* **16**, 3396 (2025).
- [45] A. González-Tudela and J. I. Cirac, Exotic quantum dynamics and purely long-range coherent interactions in dirac conelike baths, *Physical Review A* **97**, 043831 (2018).
- [46] J. Redondo-Yuste, M. B. de Paz, P. A. Huidobro, and A. González-Tudela, Quantum electrodynamics in anisotropic and tilted dirac photonic lattices, *New Journal of Physics* **23**, 103018 (2021).
- [47] Z.-X. Gong, M. F. Maghrebi, A. Hu, M. L. Wall, M. Foss-Feig, and A. V. Gorshkov, Topological phases with long-range interactions, *Physical Review B* **93**, 041102 (2016).
- [48] Z.-X. Gong, M. F. Maghrebi, A. Hu, M. Foss-Feig, P. Richerme, C. Monroe, and A. V. Gorshkov, Kaleidoscope of quantum phases in a long-range interacting spin-1 chain, *Physical Review B* **93**, 205115 (2016).
- [49] B. Žunkovič, M. Heyl, M. Knap, and A. Silva, Dynamical quantum phase transitions in spin chains with

- long-range interactions: Merging different concepts of nonequilibrium criticality, [Physical review letters](#) **120**, 130601 (2018).
- [50] R. Islam, C. Senko, W. C. Campbell, S. Korenblit, J. Smith, A. Lee, E. Edwards, C.-C. Wang, J. Freericks, and C. Monroe, Emergence and frustration of magnetism with variable-range interactions in a quantum simulator, [science](#) **340**, 583 (2013).
 - [51] E. Sánchez-Burillo, D. Porras, and A. González-Tudela, Limits of photon-mediated interactions in one-dimensional photonic baths, [Phys. Rev. A](#) **102**, 013709 (2020).
 - [52] N. W. Ashcroft and N. D. Mermin, *Solid state physics* (Holt, Rinehart and Winston, New York, NY, 1976).
 - [53] F. Bloch, Über die Quantenmechanik der Elektronen in Kristallgittern, [Z. Physik](#) **52**, 555 (1929).
 - [54] L. Chen, T. Mazaheri, A. Seidel, and X. Tang, The impossibility of exactly flat non-trivial Chern bands in strictly local periodic tight binding models, [J. Phys. A: Math. Theor.](#) **47**, 152001 (2014).
 - [55] H. C. Po, H. Watanabe, and A. Vishwanath, Fragile topology and wannier obstructions, [Phys. Rev. Lett.](#) **121**, 126402 (2018).
 - [56] S. Bravyi, D. P. DiVincenzo, and D. Loss, Schrieffer-Wolff transformation for quantum many-body systems, [Annals of Physics](#) **326**, 2793 (2011).
 - [57] A. Youssefi, S. Kono, A. Bancora, M. Chegnizadeh, J. Pan, T. Vovk, and T. J. Kippenberg, Topological lattices realized in superconducting circuit optomechanics, [Nature](#) **612**, 666 (2022).
 - [58] A. Youssefi, A. Motavassal, S. Kono, S. A. Jafari, and T. J. Kippenberg, Realization of tilted dirac-like microwave cone in superconducting circuit lattices, [arXiv:2501.10434](#) (2025).
 - [59] U. Vool and M. Devoret, Introduction to quantum electromagnetic circuits, [International Journal of Circuit Theory and Applications](#) **45**, 897 (2017).
 - [60] A. Ramachandran, A. Andreanov, and S. Flach, Chiral flat bands: Existence, engineering, and stability, [Phys. Rev. B](#) **96**, 161104 (2017).
 - [61] P. W. Anderson, Absence of Diffusion in Certain Random Lattices, [Phys. Rev.](#) **109**, 1492 (1958).

Supplementary Material: Emergent cavity-QED dynamics along the edge of a photonic lattice

Enrico Di Benedetto ¹ Xuejian Sun,^{2,1,*} Marcel A. Pinto ¹ Luca Leonforte ¹ Chih-Ying Chang ^{3,4}
Vincent Jouanny ^{3,4} Léo Peyruchat ^{3,4} Pasquale Scarlino ^{3,4} and Francesco Ciccarello ^{1,5}

¹*Università degli Studi di Palermo, Dipartimento di Fisica e Chimica – Emilio Segrè, via Archirafi 36, I-90123 Palermo, Italy*

²*School of Physics and Telecommunication Engineering,*

Zhoukou Normal University, 466001 Zhoukou, China

³*Hybrid Quantum Circuits Laboratory (HQC), Institute of Physics,
École Polytechnique Fédérale de Lausanne (EPFL), 1015, Lausanne, Switzerland*

⁴*Center for Quantum Science and Engineering,
Institute of Physics, École Polytechnique Fédérale de Lausanne (EPFL), 1015, Lausanne, Switzerland*

⁵*NEST, Istituto Nanoscienze-CNR, Piazza S. Silvestro 12, 56127 Pisa (Italy)*

(Dated: July 21, 2025)

CONTENTS

I. Normal modes of the lattice Hamiltonian H_B	9
A. Mapping to uncoupled Rice-Mele models	9
B. Bulk modes	10
C. Edge modes	10
II. Properties of the flat band of edge modes	10
III. Derivation of the effective cavity-QED model	11
A. Markovian master equation: brief review	11
B. Single-qubit master equation	12
C. Many-qubit master equation	13
IV. Matrix elements of the decay rate matrix	14
A. Calculation of $\gamma_{ii}(\Delta)$	14
B. Calculation of $\gamma_{i \neq j}(\Delta)$	15
V. Exact solution of the dissipative Jaynes-Cummings model	16
VI. Resonant State-transfer dynamics in a two qubit system	17
VII. Flat band projection operator: relevant matrix elements	18
VIII. Shape of the effective cavity modes	19
IX. Qubit-qubit interaction potential in the dispersive regime	19
X. Experimental Implementation	21

* Correspondence email address: Xuejian890@gmail.com

I. NORMAL MODES OF THE LATTICE HAMILTONIAN H_B

Pristine graphene has the structure of a composite 2D triangular Bravais lattice [52]. A lattice site (resonator) has position given by $\mathbf{R}_\nu = n\mathbf{e}_1 + m\mathbf{e}_2 + \mathbf{d}_\nu$, where (n, m) are integers while

$$\mathbf{e}_1 = a\sqrt{3}\left(\frac{\sqrt{3}}{2}, \frac{1}{2}\right), \quad \mathbf{e}_2 = a\sqrt{3}(0, 1), \quad \mathbf{d}_\nu = \nu a\left(\frac{1}{2}, \frac{\sqrt{3}}{2}\right) \quad (11)$$

are respectively primitive vectors ($\mathbf{e}_{1(2)}$) and basis vectors (\mathbf{d}_ν) with $\nu = 0, 1$ the sublattice index, and where a is distance between nearest-neighbour resonators defined as $a = |\mathbf{R}_1 - \mathbf{R}_0|$. This entails e.g. that $|\mathbf{e}_1| = a\sqrt{3}$, corresponding to the distance between unit cells located at (n, m) and $(n \pm 1, m)$ (same goes for $|\mathbf{e}_2|$). Sublattice $\nu=0$ ($\nu=1$) corresponds to the a - (b -) sublattice in the main text.

The reciprocal lattice has primitive vectors

$$\mathbf{b}_1 = 2\pi \frac{\mathbf{Q} \cdot \mathbf{e}_2}{\mathbf{e}_1 \cdot \mathbf{Q} \mathbf{e}_2} = \frac{2\pi}{V} a\sqrt{3}(1, 0), \quad \mathbf{b}_2 = 2\pi \frac{\mathbf{Q} \mathbf{e}_1}{\mathbf{e}_2 \cdot \mathbf{Q} \mathbf{e}_1} = \frac{2\pi}{V} a\sqrt{3}\left(-\frac{1}{2}, \frac{\sqrt{3}}{2}\right), \quad (12)$$

where $V = |\mathbf{e}_1 \cdot \mathbf{Q} \mathbf{e}_2| = a^2 3\sqrt{3}/2$ is the volume of the primitive unit cell and \mathbf{Q} is the 2×2 matrix describing a counter-clockwise $\frac{\pi}{2}$ rotation on the xy plane. In the following, we will set $a = 1$ and assume N_1 (N_2) unit cells along the \mathbf{e}_1 (\mathbf{e}_2) direction.

Based on the above, the Hamiltonian H_B [see Eq.(1) in the main text] with a zigzag edge embodied by all cells having $n = 0$ can be conveniently arranged as

$$H_B = \sum_m h_B(m) \quad (13)$$

with

$$h_B(m) = \delta \sum_{n=0}^{N_1-1} \left(a_{nm}^\dagger a_{nm} - b_{nm}^\dagger b_{nm} \right) + J \sum_{n=1}^{N_1-1} (\beta a_{n+1m} + a_{nm} + a_{nm+1}) b_{nm}^\dagger + \text{H. c.}, \quad (14)$$

which holds even in the case of an anisotropic lattice specified by the parameter β . The thermodynamic limit discussed in the main text is obtained for $N_1, N_2 \rightarrow \infty$.

We next review how to map the lattice Hamiltonian H_B into a set of uncoupled 1D Rice-Mele models [24], which dramatically simplifies the calculation of its normal modes and spectrum.

A. Mapping to uncoupled Rice-Mele models

While the edge enforces a hard-wall boundary condition along the direction \mathbf{e}_1 , the direction \mathbf{e}_2 (along the edge) has no boundaries and we can accordingly enforce periodic boundary conditions (BCs). Along the latter direction, the lattice is therefore translationally invariant allowing to take advantage of the Bloch theorem [53]. Accordingly, we perform a partial Fourier-transform of real-space bosonic ladder operators defined by

$$a_{nm} = \frac{1}{\sqrt{2\pi}} \sum_k e^{i[km + \phi_a(n)]} a_{kn}, \quad b_{nm} = \frac{1}{\sqrt{2\pi}} \sum_k e^{i[km + \phi_b(n)]} b_{kn}, \quad (15)$$

where $\phi_a(n) = n/2$ and $\phi_b(n) = (n+1)/2$ are n -dependent phase factors, which are introduced so as to ensure that the transformed Hamiltonian features only real matrix elements. Operators a_{kn} and b_{kn} fulfill bosonic commutation rules. Substituting this expression for the cavity ladder operators in Eq. (13), after some lengthy algebra, the bath Hamiltonian can be decomposed as $H_B = \sum_k \mathcal{H}_k$, where

$$\mathcal{H}_k = \delta \sum_{n=0}^{\infty} \left(a_{kn}^\dagger a_{kn} - b_{kn}^\dagger b_{kn} \right) + J \sum_{n=0}^{\infty} \left[\beta a_{kn+1} b_{kn}^\dagger + 2 \cos\left(\frac{k}{2}\right) a_{kn} b_{kn}^\dagger + \text{H. c.} \right]. \quad (16)$$

Thus, the model is mapped into a collection of uncoupled 1D Rice-Mele models: each is labeled by k and features an inter-cell hopping rate βJ and a k -dependent intra-cell hopping rate $\mathcal{J}_k = 2J \cos \frac{k}{2}$. The diagonalization of H_B thereby reduces to the diagonalization of \mathcal{H}_k , which is carried out next first for bulk modes and then for edge modes.

B. Bulk modes

Under periodic BCs, the bulk spectrum of \mathcal{H}_k is worked out as

$$\omega_{\pm}(k, q) = \pm \sqrt{\delta^2 + (\beta J)^2 + \mathcal{J}_k^2 + 2\beta J \mathcal{J}_k \cos q} = \pm J \omega(k, q) \quad (17)$$

where $0 \leq q \leq 2\pi$. The normal mode corresponding to frequency $\omega_{\pm}(k, q)$ reads

$$B_{\pm}(k, q) = \frac{\mathcal{N}_{\pm}(k, q)}{\sqrt{2\pi}} \sum_n \left[\left(2 \cos \frac{k}{2} + \beta e^{-iq} \right) e^{-iqn} a_{kn} \pm (\omega(k, q) \mp (\delta/J)) e^{-iqn} b_{kn} \right] \quad (18)$$

where $[\mathcal{N}_{\pm}(k, q)]^{-2} = 2\omega(k, q)[\omega(k, q) \mp (\delta/J)]$ is a normalization constant. Exploiting the definition of the a_{kn}, b_{kn} operators given in Eq. (15), $B_{\pm}(k, q)$ can be expressed in real space as

$$B_{\pm}(k, q) = \frac{\mathcal{N}_{\pm}(k, q)}{2\pi} \sum_{n,m} \left[\left(2 \cos \frac{k}{2} + \beta e^{-iq} \right) e^{-ik(m+n/2)} e^{-iqn} a_{nm} \pm (\omega(k, q) \mp (\delta/J)) e^{-ik(m+n/2+1/2)} e^{-iqn} b_{nm} \right]. \quad (19)$$

The above bulk modes are valid under *periodic* BCs. For *open* BCs, which are those of concern here, the bulk spectrum of \mathcal{H}_k in Eq. (17) still holds while normal modes can be constructed from those under PBCs as the superposition $\mathcal{B}_{\pm}(k, q) = [B_{\pm}(k, 2\pi - q) - B_{\pm}(k, q)]/\sqrt{2}i$ where now $0 \leq q \leq \pi$. This yields

$$\mathcal{B}_{\pm}(k, q) = \mathcal{N}_{\pm}(k, q) \frac{2}{\sqrt{\pi}} \sum_{n=0}^{\infty} \left[\left(2 \cos \frac{k}{2} \sin q(n+1) + \beta \sin qn \right) a_{kn} \pm (\omega(k, q) \mp (\delta/J)) \sin q(n+1) b_{kn} \right], \quad (20)$$

which can be again expressed in real space using Eq. (15).

C. Edge modes

In the gapless case i.e., for $\delta=0$, Hamiltonian \mathcal{H}_k reduces to a k -dependent SSH Hamiltonian [24]. Accordingly, for $|\mathcal{J}_k| < \beta|J|$, which in the present context corresponds to the condition

$$2 \arccos \frac{\beta}{2} \leq |k| < \pi \quad (21)$$

zero-frequency edge modes appear under open BCs. Those lying on the left edge read [15] (recall that our lattice is semi-infinite)

$$\mathcal{E}_k = \mathcal{N}_k \sum_n (-1)^n e^{-n/\lambda_k} a_{kn} \quad (22)$$

with $\lambda_k^{-1} = \ln |\beta J / \mathcal{J}_k|$ and $\mathcal{N}_k = \sqrt{-[2/\beta^2 - 1 + (2/\beta^2) \cos k]}$. In real space, edge modes \mathcal{E}_k read

$$\mathcal{E}_k = \frac{\mathcal{N}_k}{\sqrt{2\pi}} \sum_{n=0}^{\infty} \sum_m (-1)^n e^{-ik(m+n/2)} e^{-n/\lambda_k} a_{nm}, \quad (23)$$

showing that λ_k embodies a k -dependent penetration length. as expected having a non-zero envelope only on the a -sublattice.

In the gapped case i.e., for $\delta \neq 0$, edge modes will also appear, having the same expression in real space given by (23). The only difference is their energy, now equal to δ i.e., the value of the on-site energy of cavities in the a -sublattice.

II. PROPERTIES OF THE FLAT BAND OF EDGE MODES

The frequency-degenerate edge modes \mathcal{E}_k represent a *flat band* (FB) of frequency δ . A major property of standard FBs is that the corresponding subspace can be spanned through a basis of compact localized modes i.e., modes

strictly localized in a finite region of space [19]. This property relies crucially on two assumptions, namely the fact that the FB has support on the full BZ and it is topologically trivial [54]. Our edge modes \mathcal{E}_k , however, form a *partial* FB since their support (21) is *shorter* than the BZ for $\beta < 2$. In general, as shown in Ref. [18], this is enough to prevent the construction of a properly-defined set of compact states spanning the FB subspace. On the other hand, when $\beta \geq 2$ the edge modes form a *full* FB spanning the whole BZ. Thus, one might wonder whether in this case it is instead possible to span the FB subspace using a basis of compact states. We show next that, unlike standard full FBs, this is not possible in the system under study.

Assuming $\beta \geq 2$ (full FB), we can follow a general procedure (see e.g. Ref. [21] and references therein) which allows to construct a compact mode ϕ_{m_0} localized around resonator $m = m_0$ along the zigzag edge ($n = 0$) as

$$\phi_{m_0} = \frac{1}{\sqrt{2\pi}} \int_{-\pi}^{\pi} dk \sqrt{F(k)} e^{ikm_0} \mathcal{E}_k, \quad (24)$$

where function $F(k)$ is required to fulfill $F(k) = |\mathcal{N}_k|^{-2}$ with \mathcal{N}_k the normalization constant appearing in the definition of the edge modes \mathcal{E}_k [see Eq. (23)]. In real space, using Eq. (23), ϕ_{m_0} reads

$$\phi_{m_0} = \sum_{n,m} \frac{(-1)^n}{\beta^{n+1}} \varphi(n, m - m_0) a_{nm} \quad \text{with} \quad \varphi(n, m) = \frac{1}{2\pi} \int_{-\pi}^{\pi} dk \left(2 \cos \frac{k}{2} \right)^n e^{-ik(n+m)}. \quad (25)$$

This last expression is in fact the Fourier transform of $(\mathcal{J}_k/J)^n$, which can be computed easily with the help of the following identities

$$\cos^n(\theta) = \begin{cases} \frac{1}{2^{n-1}} \sum_{r=0}^{r < 2n} \binom{n}{2r} \cos[(2r-n)\theta], & \text{odd } n \\ \frac{1}{2^n} \binom{n}{n/2} + \frac{1}{2^{n-1}} \sum_{r=0}^{r < 2n} \binom{n}{2r} \cos[(2r-n)\theta], & \text{even } n \end{cases}. \quad (26)$$

Using these, function $\varphi(n, m)$ can be expressed as

$$\varphi(n, m) = \begin{cases} \frac{1}{2} \sum_{r=0}^{2r < n} \binom{n}{2r} \delta_{r+2m,0}, & \text{odd } n \\ \binom{n}{n/2} \delta_{n+m,0} + \frac{1}{2} \sum_{r=0}^{2r < n} \binom{n}{2r} \delta_{r+2m,0}, & \text{even } n \end{cases}. \quad (27)$$

This shows that state ϕ_{m_0} cannot be compact since, for any fixed n , its amplitude is non zero on $\sim n$ resonators. For the same reason, ϕ_{m_0} is not normalizable in the thermodynamic limit.

Thus, it is not possible in this case, even when the FB has support on the full BZ and is gapped from the bulk spectrum (if $\beta > 2$), to span the FB subspace through basis of compact localized modes. This impossibility is a consequence of topology, known as *Wannier obstruction*, which prevents to construct localized Wannier functions using eigenmodes of topologically non-trivial bands [18, 55].

For technical convenience, in the remainder we will often make use of a single-photon Dirac formalism such that, in particular, $|a_{n,m}\rangle = a_{nm}^\dagger |\text{vac}\rangle$ (with $|\text{vac}\rangle$ the field's vacuum) denotes the Fock state where resonator $a_{n,m}$ is populated by a single photon. Likewise, $|\mathcal{E}_k\rangle = \mathcal{E}_k^\dagger |\text{vac}\rangle$ and $|\mathcal{B}_\pm^\dagger(k, q)\rangle = \mathcal{B}_\pm^\dagger(k, q) |\text{vac}\rangle$ are single-photon edge and bulk states, respectively.

III. DERIVATION OF THE EFFECTIVE CAVITY-QED MODEL

A. Markovian master equation: brief review

Let an open system S be in contact with a bath B with an interaction Hamiltonian of the form $H_{\text{SB}}(t) = \sum_i X_i(t) \otimes E_i(t)$ (in the interaction picture), where X_i (E_i) are operators on S (B). Introducing operators $\Pi(\varepsilon)$ each of which projects S onto the eigenspace of energy ε , one can expand X_i as $X_i(\omega) = \sum_{\varepsilon' - \varepsilon = \omega} \Pi(\varepsilon) X_i \Pi(\varepsilon')$. Hence, the interaction Hamiltonian can be expressed as

$$H_{\text{SB}}(t) = \sum_{i,\omega} e^{-i\omega t} X_i(\omega) \otimes E_i(t) = \sum_{i,\omega} e^{i\omega t} X_i^\dagger(\omega) \otimes E_i^\dagger(t). \quad (28)$$

Next, starting from the Redfield master equation and performing the Markov and weak-coupling approximations, one obtains the integro-differential equation for the reduced density matrix of S [28]

$$\frac{d}{dt} \rho_S = - \int_0^\infty ds \text{Tr}_B [H_{\text{SB}}(t), [H_{\text{SB}}(t-s), \rho_S(t) \otimes \rho_B]], \quad (29)$$

where Tr_B stands for the partial trace over B . Substituting (28) and keeping only slowly-rotating terms corresponding to nearly-resonant bath modes, one ends up with the master equation

$$\frac{d}{dt}\rho_S(t) = \sum_{ij} \sum_{\omega} \Gamma_{ij}(\omega) \left[X_j(\omega) \rho_S(t) X_i^\dagger(\omega) - X_i^\dagger(\omega) X_j(\omega) \rho_S(t) \right] + \text{H. c.}, \quad (30)$$

where ω is the characteristic frequency of S while matrix $\Gamma_{ij}(\omega)$ is given by

$$\Gamma_{ij}(\omega) = \int_0^\infty ds e^{i\omega s} \text{Tr}_B E_i^\dagger(t) E_j(t-s) \rho_B \equiv \frac{1}{2} \gamma_{ij}(\omega) + i S_{ij}(\omega). \quad (31)$$

The real part of this matrix describe the irreversible decay rate into the bath, while the imaginary part renormalizes the free Hamiltonian of S .

B. Single-qubit master equation

The Hamiltonian of the total system can be rearranged as

$$H = H_{\text{JC}} + \Delta \sigma^\dagger \sigma + \sum_{k,q,\mu} \omega_\mu(k,q) \mathcal{B}_\mu^\dagger(k,q) \mathcal{B}_\mu(k,q) + g \sum_{k,q} \sum_{\mu=\pm} \left(f_\mu(k,q) \mathcal{B}_\mu^\dagger(k,q) \sigma + \text{H. c.} \right), \quad (32)$$

where

$$H_{\text{JC}} = g \sum_{|k|>t} \left(\frac{\mathcal{N}_k}{\sqrt{2\pi}} \mathcal{E}_k \sigma^\dagger + \text{H. c.} \right) \quad (33)$$

is the coupling Hamiltonian describing the interaction between the qubit and all edge modes $\{\mathcal{E}_k\}$. Here, $t = 2 \arccos \beta$ and $\varepsilon_k(0,0) = \mathcal{N}_k / \sqrt{2\pi}$ is the amplitude of the edge mode \mathcal{E}_k at site a_{00} to which the atom is coupled. Also, $f_\pm(k,q) = \langle a_{00} | \mathcal{B}_\pm(k,q) \rangle$ is the amplitude of the bulk mode $\mathcal{B}_\pm(k,q)$ at the resonator coupled to the emitter, reading

$$f_\pm(k,q) = \frac{1}{\pi} \mathcal{N}_\pm(k,q) \left[2 \cos \frac{k}{2} \sin q \right] = \frac{\sqrt{2} \cos \frac{k}{2} \sin q}{\pi [\omega(k,q)]^2} \quad (34)$$

in the $\delta=0$ case. Since f turns out to be independent of the band index μ , we will drop such index in the rest of this derivation.

The Hamiltonian H_{JC} can be arranged as [cf. Eq. (4) in the main text]

$$H_{\text{JC}} = g \left[\sigma^\dagger \left(\sum_{|k|>t} \frac{\mathcal{N}_k}{\sqrt{2\pi}} \mathcal{E}_k + \text{H. c.} \right) \right] \equiv \Omega \left(\sigma^\dagger \mathcal{C} + \text{H. c.} \right), \quad (35)$$

where $\Omega = g / \sqrt{A}$ and we have introduced a *superposition mode* \mathcal{C} [cf. Eq. (6) therein] such that

$$\mathcal{C} = \sqrt{A} \sum_{|k|>t} \frac{\mathcal{N}_k}{\sqrt{2\pi}} \mathcal{E}_k = \sqrt{A} \sum_{nm} c(n,m) a_{nm}. \quad (36)$$

In this expression, $c(n,m)$ is the amplitude of the mode in real space (which will be computed in a particular case in [section VII](#)) and A plays the role of a normalization constant, which can be computed e.g. by requiring that $[\mathcal{C}, \mathcal{C}^\dagger] = 1$ i.e., that the mode obeys bosonic commutation rules. From this, one sees that

$$[\mathcal{C}, \mathcal{C}^\dagger] = \mathcal{A} \frac{1}{2\pi} \sum_{|k|>t} |\mathcal{N}_k|^2 \rightarrow \mathcal{A} \frac{1}{\pi} \int_t^\pi dk \sqrt{-[2/\beta^2 - 1 + (2/\beta^2) \cos k]}, \quad (37)$$

which always converges (regardless of β) in the thermodynamic limit (the precise value is discussed in [section VII](#)). We stress that, due to the normalization of the emergent mode \mathcal{C} , the coupling strength to this mode remains finite in the thermodynamic limit. This takes care of the interaction with the edge modes.

Regarding the bulk modes, these can be treated as an effective bosonic reservoir to which the qubit is coupled to within the Born-Markov approximation. This can be justified by looking at the local density-of-states of such modes on the resonator a_{00} . Indeed, recall that we are interested in frequencies nearly-resonant with the FB at $\Delta = 0$, which on the other hand is resonant with the Dirac point emerging from the bulk modes dispersion law [see Eq. (17)]. Around this point, it is well known [27] that the density-of-states of graphene bulk modes scale linearly with their energy, being exactly zero on resonance with the Dirac point i.e., at $\Delta = 0$. This means that, since light-matter coupling is indeed proportional to said density, the interaction with bulk modes will be much weaker than the one with the FB of edge modes.

Having said that, replacing in Eq. (31) $\omega = \Delta$, $X_1 = X_2^\dagger = \sigma$ and $E_1 = E_2^\dagger = g \sum_{k,q,\mu} f(k,q)$ yields

$$\Gamma_{ij}(\Delta) = \delta_{ij} \delta_{i1} g^2 \sum_{k,q} \sum_{\mu=\pm} |f(k,q)|^2 \int_0^\infty ds e^{i(\Delta - \omega_\mu(k,q))s}, \quad (38)$$

hence

$$\gamma(\Delta) = 2\pi g^2 \sum_{k,q} \sum_{\mu=\pm} |f(k,q)|^2 \delta(\Delta - \omega_\mu(k,q)) \quad (39)$$

while (due to the symmetries of the integrand) $S_{ij}(\Delta) = 0$. Going back to the Schrödinger picture, this leads to master equation (5) in the main text.

C. Many-qubit master equation

The derivation described in the last section can be generalized to the case of N_q qubits as follows. The interaction Hamiltonian of the qubits with the FB of edge modes can be arranged as

$$H_{JC} = g \sum_j \left(\sigma_j \tilde{\mathcal{C}}_j^\dagger + \text{H.c.} \right), \quad (40)$$

where each ladder operator $\tilde{\mathcal{C}}_j$ (one for each qubit j) has the same expression as \mathcal{C} (apart from the normalization factor) in the single-qubit case with $m \rightarrow m - m_j$.

These N_q modes, however, overlap one another and, most importantly, they are not orthogonal. As such, $[\tilde{\mathcal{C}}_i, \tilde{\mathcal{C}}_j^\dagger] \neq \delta_{ij}$. To end up with a well-defined set of N_q modes fulfilling bosonic commutation rules, following Ref. [20] we perform a transformation defined by the $N_q \times N_q$ invertible matrix \mathbf{M} such that $\mathbf{M}\mathbf{M}^\dagger = \mathbf{P}$, where \mathbf{P} is the same as in Section VII. Modes $\{\tilde{\mathcal{C}}_j\}$ are transformed into

$$\mathcal{C}_i = \sum_j (M^{-1})_{ij} \tilde{\mathcal{C}}_j, \quad (41)$$

which now fulfill $[\mathcal{C}_i, \mathcal{C}_j^\dagger] = \delta_{ij}$. The interaction Hamiltonian (40) in terms of the new commuting modes reads

$$H_{JC} = g \sum_{ij} \left(\sigma_i M_{ij} \mathcal{C}_i^\dagger + \text{H.c.} \right). \quad (42)$$

On the other hand, the bulk modes can be traced out using the same procedure as before. Notice that in this case, though, each $f(k,q)$ acquires a k -dependent phase, depending on the atom position m_i . Proceeding as before, the master equation in Schrödinger picture reads

$$\frac{d}{dt} \rho_S = -i \left[\Delta \sum_i \sigma_i^\dagger \sigma_i + g \sum_{ij} \left(\mathcal{C}_i M_{ij} \sigma_j^\dagger + \text{H.c.} \right), \rho_S \right] + \sum_{ij} \gamma_{ij}(\Delta) \left[\sigma_j \rho_S \sigma_i^\dagger - \frac{1}{2} \{ \sigma_i^\dagger \sigma_j, \rho_S \} \right], \quad (43)$$

where the matrix of decay rates γ_{ij} reads

$$\gamma_{ij}(\omega) = 2\pi g^2 \sum_{k,q,\mu} |f(k,q)|^2 \cos(k|m_i - m_j|) \delta(\omega - \omega_\mu(k,q)). \quad (44)$$

As expected, the diagonal elements of this matrix coincides with the single-qubit decay rate while the off-diagonal terms will feature an addition $\cos k|m_i - m_j|$ term. Notice that this master equation is a valid description of the system as long as the qubits are *close* to each other, so as to neglect effects due to the time-delay in the light propagation.

IV. MATRIX ELEMENTS OF THE DECAY RATE MATRIX

In this section, we focus on the computation of the matrix elements of matrix γ . For the sake of simplicity, we restrict ourselves to the case $\beta \leq 2$ i.e., when the FB is not gapped from the rest of the spectrum.

A. Calculation of $\gamma_{ii}(\Delta)$

In the thermodynamic limit, one can express the single qubit decay rate or, equivalently, the element $\gamma_{ii}(\Delta)$ in the dissipation matrix arising from the two qubit master equation as

$$\frac{\gamma_{ii}(\Delta)}{g^2} = \frac{8}{\pi} \int_0^\pi dq \int_{-\pi}^\pi dk \frac{\cos^2(k/2) \sin^2(q)}{\beta^2 + 4\beta \cos(k/2) \cos q + 4 \cos^2(k/2)} \sum_\mu \delta(\Delta - \omega_\mu(k, q)). \quad (45)$$

Now, since

$$\sum_\mu \delta(\Delta - \omega_\mu(k, q)) = 2|\Delta| \delta(\Delta^2 - J^2[\omega(k, q)]^2), \quad (46)$$

one can simplify the μ dependency and also to conclude that the denominator is proportional to $(\Delta/J)^2$. Thus

$$\frac{\gamma_{ii}(\Delta)}{g^2} = \frac{32J^2}{\pi|\Delta|} \int_0^\pi dq \int_0^\pi dk \cos^2(k/2) \sin^2(q) \delta(\Delta^2 - J^2[\omega(k, q)]^2). \quad (47)$$

Changing $x = \cos q$ and $y = \cos k/2$, we get that

$$\begin{aligned} \frac{\gamma_{ii}(\Delta)}{g^2} &= \frac{64J^2}{\pi|\Delta|} \int_{-1}^1 dx \int_0^1 dy \frac{y^2}{\sqrt{1-y^2}} \sqrt{1-x^2} \delta\left(4\beta J^2 y \left(x - \left[\frac{\Delta^2/J^2 - \beta^2 - 4y^2}{4\beta y}\right]\right)\right) = \\ &= \frac{16}{\beta\pi|\Delta|} \int_{-1}^1 dx \int_0^1 dy \frac{y}{\sqrt{1-y^2}} \sqrt{1-x^2} \delta\left(x - \left[\frac{\Delta^2/J^2 - \beta^2 - 4y^2}{4\beta y}\right]\right) = \\ &= \frac{4}{\beta^2\pi|\Delta|} \int_{c_0}^{c_1} dy \sqrt{\frac{16\beta^2 y^2 - [\Delta^2/J^2 - \beta^2 - 4y^2]^2}{1-y^2}}, \end{aligned} \quad (48)$$

where c_0, c_1 depends on the values of $|\Delta|/J$ and β . In particular, one finds that

$$0 < \frac{|\Delta|}{J} \leq 1 : \begin{cases} \beta < |\Delta|/J & c_0 = (|\Delta|/J - \beta)/2, & c_1 = (|\Delta|/J + \beta)/2 \\ |\Delta|/J \leq \beta \leq 2 - |\Delta|/J & c_0 = (\beta - |\Delta|/J)/2, & c_1 = (|\Delta|/J + \beta)/2 \\ \beta > 2 - |\Delta|/J & c_0 = (\beta - |\Delta|/J)/2, & c_1 = 1 \end{cases} \quad (49)$$

$$\frac{|\Delta|}{J} > 1 : \begin{cases} \beta < 2 - |\Delta|/J & c_0 = (|\Delta|/J - \beta)/2, & c_1 = (|\Delta|/J + \beta)/2 \\ 2 - |\Delta|/J \leq \beta \leq |\Delta|/J & c_0 = (|\Delta|/J - \beta)/2, & c_1 = 1 \\ \beta > |\Delta|/J & c_0 = (\beta - |\Delta|/J)/2, & c_1 = 1 \end{cases}$$

Since we are interested in the dynamics of qubits quasi-resonant to the FB, we will focus in the following in the case $0 < |\Delta|/J \leq 1$. In this limit, provided that $|\Delta|/J \leq \beta \leq 2 - |\Delta|/J$, we can simplify the integral bounds by making the substitution $y = \frac{\beta + |\Delta|t/J}{2}$ from which

$$\frac{\gamma_{ii}(\Delta)}{g^2} = \frac{4|\Delta|}{\pi\beta^2 J^2} \int_{-1}^1 dt \sqrt{\frac{\left[1 - \left(J^{\frac{1-\beta}{\Delta}} + t\right)^2\right] \left[(1 + \beta + \Delta t/J)^2 - (\Delta/J)^2\right]}{(2 + \beta + \Delta t/J)(2 - \beta - \Delta t/J)}}. \quad (50)$$

For $\Delta \simeq 0$, we can approximate the integral, yielding

$$\frac{\gamma_{ii}(\Delta)}{g^2} \simeq \frac{8|\Delta|}{\beta\pi J^2 \sqrt{4 - \beta^2}} \int_{-1}^1 dt \sqrt{1 - t^2} = \frac{4|\Delta|}{\beta J^2 \sqrt{4 - \beta^2}}. \quad (51)$$

Setting $\beta = 1$ yields the expression of the single qubit decay rate discussed in the main text.

Notice that this expression would yield a divergent decay rate for $\beta \rightarrow 0^+$ or $\beta \rightarrow 2^-$. These two limits, though, are out of the validity region of such approximation for any non-zero value of Δ . As a matter of fact, both limits have clear physical interpretation. For instance, if $\beta = 0$ then the Hamiltonian reduces to a collection of 1D homogeneous chains (stretching along the \mathbf{e}_2 direction), parametrized by n . In this case, we expect γ_{ii} to reduce to the standard decay rate into a cosine band. This is easily checked as in this case $\omega(k, q) = 2J \cos(k/2)$ and so

$$\begin{aligned} \frac{\gamma_{ii}(\Delta)}{g^2} &= \frac{2}{\pi} \int_{-\pi}^{\pi} dk [\delta(\Delta - 2J \cos(k/2)) + \delta(\Delta + 2J \cos(k/2))] \int_0^{\pi} dq \sin^2(q) = \\ &= \int_{-\pi}^{\pi} dk [\delta(\Delta - 2J \cos(k/2)) + \delta(\Delta + 2J \cos(k/2))] \equiv \int_{-\pi}^{\pi} dk \delta(\Delta - 2J \cos(k)), \end{aligned} \quad (52)$$

yielding the expected result according to Fermi Golden Rule. On the other hand, in the $\beta = 2$ limit, the Dirac cone spectral shape is modified becoming a so-called *semi-Dirac* cone [46], whose dispersion law is linear in one quasi-momentum component and quadratic in the other. For this reason, we expect γ_{ii} to be smaller in this case than its value for $\beta < 2$. This intuition is verified by numerically computing the integral and it is shown in Fig. 3(e).

B. Calculation of $\gamma_{i \neq j}(\Delta)$

In the same way as before, one would like to compute

$$\frac{\gamma_{ij}(\Delta)}{g^2} = \frac{8}{\pi} \int_0^{\pi} dq \int_{-\pi}^{\pi} dk \frac{\cos^2(k/2) \sin^2(q)}{\beta^2 + 4\beta \cos(k/2) \cos q + 4 \cos^2(k/2)} \cos k(m_i - m_j) \sum_{\mu} \delta(\Delta - \omega_{\mu}(k, q)). \quad (53)$$

Doing the same simplifications as before, this integral is written as

$$\frac{\gamma_{ij}(\Delta)}{g^2} = \frac{32J^2}{\pi|\Delta|} \int_0^{\pi} dq \int_0^{\pi} dk \cos^2(k/2) \sin^2(q) \cos(k|m_i - m_j|) \delta(\Delta^2 - J^2[\omega(k, q)]^2). \quad (54)$$

The previous calculation suggests to use the substitution $x = \cos q$ and $y = \cos k/2$. In order to do so, one recalls that

$$\cos n\theta = \sum_{r=0}^{2r \leq n} (-1)^r \binom{n}{2r} \cos^{n-2r}(\theta) \sin^{2r}(\theta) \quad (55)$$

and using this, it is possible to write

$$\frac{\gamma_{ij}(\Delta)}{g^2} = \frac{4}{\beta^2 \pi |\Delta|} \sum_{r=0}^{r \leq |m_i - m_j|} (-1)^r \binom{2|m_i - m_j|}{2r} \int_{c_0}^{c_1} dy \sqrt{16\beta^2 y^2 - [\Delta^2/J^2 - \beta^2 - 4y^2]^2} (1 - y^2)^{r-1/2} y^{2|m_i - m_j| - 2r} \quad (56)$$

with the same prescription about the integral limits as before. For $\Delta \simeq 0$, the integral can be approximated as

$$\begin{aligned} \frac{\gamma_{ij}(\Delta)}{g^2} &\simeq \frac{8|\Delta|}{\beta \pi J^2 \sqrt{4 - \beta^2}} \sum_{r=0}^{r \leq |m_i - m_j|} (-1)^r \binom{2|m_i - m_j|}{2r} \left(\frac{\beta}{2}\right)^{2|m_i - m_j| - 2r} \left(1 - \left(\frac{\beta}{2}\right)^2\right)^r \times \int_{-1}^1 dt \sqrt{1 - t^2} = \\ &= \frac{4|\Delta|}{\beta J^2 \sqrt{4 - \beta^2}} \cos\left(2|m_i - m_j| \arccos \frac{\beta}{2}\right). \end{aligned} \quad (57)$$

Even in this case we see that around the Dirac point, the scaling of the decay rate is linear in $|\Delta|$. Notice that in general, the matrix elements of the γ matrix depends on β in a non-monotonic way. The decay rates reach a minimum in correspondence of $\beta = \sqrt{2}$, in which case dissipation will be minimized. The same comments regarding the $\beta \rightarrow 0^+$ and $\beta \rightarrow 2^-$ limits present at the end of section IV A apply here.

V. EXACT SOLUTION OF THE DISSIPATIVE JAYNES-CUMMINGS MODEL

The master equation (5) reported in the main text describes a dissipative Jaynes-Cummings model in which – unlike standard cases – a *lossy* qubit couples to a *lossless* bosonic cavity. In a different context, the same model was already considered in Ref. [29], where a complete analytical solution in the single-excitation sector is discussed. Taking inspiration from this, here we discuss the general solution of our model, depending on the values of Δ and $\beta < 2$.

Suppose that the system is initially in the pure state $\rho = |e\rangle\langle e|$, corresponding to an initially excited qubit. At each later time, the probability of finding the qubit in its excited state can be found by solving the master equation. To do so, one notices that (5) can be rewritten as

$$\dot{\rho} = -i\left(\mathcal{H}_{\text{NH}}\rho - \rho\mathcal{H}_{\text{NH}}^\dagger\right) + \gamma(\Delta)\sigma\rho\sigma^\dagger, \quad (58)$$

where the last term is the usual recycling term and the non-Hermitian Hamiltonian reads

$$\mathcal{H}_{\text{NH}} = \left(\Delta - i\frac{\gamma(\Delta)}{2}\right)\sigma^\dagger\sigma + \Omega\left(\sigma\mathcal{C}^\dagger + \text{H.c.}\right). \quad (59)$$

Within the single-excitation sector, spanned by states $|e, \text{vac}\rangle$ and $|g, \mathcal{C}\rangle$, the matrix elements of the recycling term yields no contribution. This allows to cast the master equation into a Von-Neumann-like equation, where the dynamics is generated by the non-Hermitian Hamiltonian \mathcal{H}_{NH} . Solving this is equivalent to solving the time-dependent Schrödinger equation

$$i\frac{d}{dt}|\Psi(t)\rangle = \mathcal{H}_{\text{NH}}|\Psi(t)\rangle, \quad (60)$$

where $\rho(t) = |\Psi(t)\rangle\langle\Psi(t)|$. Writing the state of the system at a generic time t as $|\Psi(t)\rangle = c_e(t)|e, \text{vac}\rangle + C_g(t)|g, \mathcal{C}\rangle$ and solving for $c_e(t)$, we end up with the second order homogeneous linear differential equation

$$\frac{d^2}{dt^2}c_e(t) + \left(i\Delta + \frac{\gamma(\Delta)}{2}\right)\frac{d}{dt}c_e(t) + \Omega^2c_e(t) = 0, \quad (61)$$

with the boundary conditions $c_e(0) = 1$ and $\dot{c}_e(0) = -i\Delta - \gamma(\Delta)/2$. Taking $c_e(t) = e^{\lambda t}$ as an ansatz for the solution, the characteristic polynomial associated to the differential equation reads $p(\lambda) = \lambda^2 + (i\Delta + \gamma(\Delta)/2)\lambda + \Omega^2$, whose roots are

$$\lambda_{\pm} = -\frac{1}{2}\left(i\Delta + \frac{\gamma(\Delta)}{2}\right) \pm \frac{i}{2}\sqrt{4\Omega^2 - \left(i\Delta + \frac{\gamma(\Delta)}{2}\right)^2} \equiv -\frac{\mu}{2} \pm \frac{i}{2}\sqrt{4\Omega^2 - \mu^2} \quad (62)$$

with $\mu = i\Delta + \gamma(\Delta)/2$. This allows us to write the general solution as

$$c_e(t) = e^{-\mu t/2} \left[\cos\left(\frac{\sqrt{4\Omega^2 - \mu^2}}{2}t\right) - \frac{\mu}{\sqrt{4\Omega^2 - \mu^2}} \sin\left(\frac{\sqrt{4\Omega^2 - \mu^2}}{2}t\right) \right]. \quad (63)$$

We now perform some approximations. Given that we are in the weak coupling regime i.e., $g \ll J$, and since we are interested in the emerging dynamics when the qubit is (nearly-)resonant with the effective cavity mode, we can approximate

$$\sqrt{4\Omega^2 - \mu^2} \simeq \Omega_R \left[1 - \frac{i}{2} \frac{\Delta\gamma(\Delta)}{\Omega_R^2} \right], \quad \frac{1}{\sqrt{4\Omega^2 - \mu^2}} \simeq \frac{1}{\Omega_R} \left[1 + \frac{i}{2} \frac{\Delta\gamma(\Delta)}{\Omega_R^2} \right], \quad (64)$$

where $\Omega_R = \sqrt{4\Omega^2 + \Delta^2}$ is the vacuum Rabi frequency. Accordingly, the general solution can be thus approximated as

$$c_e(t) \simeq e^{-\mu t/2} \left[\cos\left(\frac{\Omega_R}{2}t\right) - \frac{\mu}{\Omega_R} \sin\left(\frac{\Omega_R}{2}t\right) + \frac{i}{2} \frac{\mu\Delta\gamma(\Delta)}{\Omega_R^3} \sin\left(\frac{\Omega_R}{2}t\right) \right]. \quad (65)$$

To leading order in g , the probability of finding the qubit in the excited state can be approximated as

$$p_e(t) = |c_e(t)|^2 \simeq e^{-\gamma(\Delta)t/2} \left[1 - \frac{4\Omega^2}{\Omega_R^2} \sin^2 \left(\frac{\Omega_R}{2} t \right) \right]. \quad (66)$$

Thus, in the weak-coupling regime, the qubit undergoes damped vacuum Rabi oscillations with oscillation frequency Ω_R and damping rate $\gamma(\Delta)$.

VI. RESONANT STATE-TRANSFER DYNAMICS IN A TWO QUBIT SYSTEM

In this section, we briefly discuss the exact solution to the dynamics of two qubits coupled to edge of *zigzag* graphene on resonance with the FB ($\Delta = 0$). In this case, the effective model in (8) would predict a purely-coherent dynamics generated by the Hamiltonian

$$\mathcal{H}_{JC} = g \sum_{j,j'=1}^2 \left(\sigma_j^\dagger M_{jj'} \mathcal{C}_{j'} + \text{H.c.} \right), \quad (67)$$

where $M_{jj'}$ is the matrix element of the 2×2 matrix \mathbf{M} defined as $\mathbf{M}\mathbf{M}^\dagger = \mathbf{P}$, being \mathbf{P} the FB projector computed at the qubits' positions. For the purpose of this section, we are not interested in the exact values of those coefficients, but it is worth noting that, as $P_{jj'}$ scales as a power-law with the distance $|m_i - m_j|$ between the emitters [see Sec. [section VII](#)], also the elements of \mathbf{M} will inherit the same scaling.

We now assume that the system is initially in state $|\Psi(0)\rangle = |e_1 g_2, \text{vac}\rangle$ i.e., first (second) qubit in the excited (ground) state and the field in the vacuum state. Thus, within the single-excitation sector, the state of the system at a generic time t reads

$$|\Psi(t)\rangle = c_{e1}(t) |e_1 g_2, \text{vac}\rangle + c_{e2}(t) |g_1 e_2, \text{vac}\rangle + c_{g1}(t) |g_1 g_2, \mathcal{C}_1\rangle + c_{g2}(t) |g_1 g_2, \mathcal{C}_2\rangle. \quad (68)$$

This allows to write down the Schrödinger equation as

$$\begin{cases} i \frac{d}{dt} c_{e1}(t) = g M_{11} c_{g1}(t) + g M_{12} c_{g2}(t) \\ i \frac{d}{dt} c_{e2}(t) = g M_{21} c_{g1}(t) + g M_{22} c_{g2}(t) \\ i \frac{d}{dt} c_{g1}(t) = g M_{11} c_{e1}(t) + g M_{12} c_{e2}(t) \\ i \frac{d}{dt} c_{g2}(t) = g M_{21} c_{e1}(t) + g M_{22} c_{e2}(t) \end{cases}, \quad (69)$$

with $c_{e1}(0) = 1$ and $c_{e2}(0) = c_{g1}(0) = c_{g2}(0) = 0$ as initial conditions. Assuming as an ansatz that $c_{ei} = A_i e^{-i\omega t}$ and $c_{gi} = \tilde{A}_i e^{-i\omega t}$, we are able to recast the problem into an eigenvalue problem, reading

$$\mathcal{M} \vec{A} = \frac{\omega}{g} \vec{A}, \quad (70)$$

where $\vec{A} = (A_1 \ A_2 \ \tilde{A}_1 \ \tilde{A}_2)^T$ and dynamical matrix is given by

$$\mathcal{M} = \begin{pmatrix} \mathbf{0}_{2 \times 2} & M \\ M^\dagger & \mathbf{0}_{2 \times 2} \end{pmatrix}, \quad (71)$$

where $\mathbf{0}$ is the zero matrix. Due to the symmetries of the problem, we have that $M_{11} = M_{22}$ and $M_{12} = M_{21}$, meaning that matrix \mathbf{M} is real and Hermitian. Now, it is clear that the eigenvalues of \mathcal{M} are

$$\omega_{1,\pm} = -g_0 \pm g_1, \quad \omega_{2,\pm} = g_0 \pm g_1, \quad (72)$$

where, for the sake of notation, we posed $g M_{11} = g_0$ and $g M_{12} = g_1$. Correspondingly, the eigenstates reads

$$\vec{v}_{1,\pm} = \frac{1}{2} (\pm 1 \ -1 \ \mp 1 \ 1)^T, \quad \vec{v}_{2,\pm} = \frac{1}{2} (\pm 1 \ 1 \ \pm 1 \ 1)^T. \quad (73)$$

In this way, we can express the solution to the Schrödinger equation as

$$\begin{cases} c_{e1}(t) = \frac{1}{4}(e^{-\omega_1-t} + e^{-\omega_1+t} + e^{-\omega_2-t} + e^{-\omega_2+t}) \\ c_{e2}(t) = \frac{1}{4}(e^{-\omega_1-t} - e^{-\omega_1+t} - e^{-\omega_2-t} + e^{-\omega_2+t}) \\ c_{g1}(t) = \frac{1}{4}(-e^{-\omega_1-t} - e^{-\omega_1+t} + e^{-\omega_2-t} + e^{-\omega_2+t}) \\ c_{g2}(t) = \frac{1}{4}(-e^{-\omega_1-t} + e^{-\omega_1+t} - e^{-\omega_2-t} + e^{-\omega_2+t}) \end{cases} . \quad (74)$$

Upon taking the squared modulus of $c_{ei}(t)$, we are able to compute the population of the two qubits as

$$P_1(t) = |c_{e1}(t)|^2 = \cos^2(g_0 t) \cos^2(g_1 t), \quad P_2(t) = |c_{e2}(t)|^2 = \sin^2(g_0 t) \sin^2(g_1 t). \quad (75)$$

This shows indeed the two qubits coherently exchange an excitation and explains also the origin of the beatings observed in Fig. 2(d-e) of the main text.

Notice that, in order to have perfect state transfer at a time $t = \tau$ i.e., $P_1(\tau) = 0$ and $P_2(\tau) = 1$, we would need $\sin^2(g_0 \tau) = 1$ and $\sin^2(g_1 \tau) = 1$. The former condition is reached at times $\tau_0 = \frac{\pi+2p\pi}{2g_0}$ while the latter corresponds to $\tau_1 = \frac{\pi+2q\pi}{2g_1}$, being $p, q \in \mathbb{Z}$. Thus, perfect state transfer is reached if, and only if,

$$p = \frac{g_0}{g_1}q + \frac{1}{2}\left(\frac{g_0}{g_1} - 1\right), \quad (76)$$

obtained from $\tau_0 = \tau_1$. We see that this equation has a solution of the integer field only if the ratio between g_0 and g_1 is commensurate i.e., $g_0/g_1 \in \mathbb{Z}$. This is not the case here, explaining why, apart from unaccounted losses in the bulk, it is not possible in this case to reach perfect state transfer. Nonetheless, still 94% fidelity can be achieved for qubits coupled to a_{00} and a_{02} , as shown in Fig. 2(d-e) of the main text.

VII. FLAT BAND PROJECTION OPERATOR: RELEVANT MATRIX ELEMENTS

The projector onto the FB subspace is defined as the operator $\mathbf{P} = \int dk |\mathcal{E}_k\rangle\langle\mathcal{E}_k|$, where k runs over the region in Eq. (21) and with $|\mathcal{E}_k\rangle = \mathcal{E}_k^\dagger |\text{vac}\rangle$ is the single-photon edge states corresponding to edge modes. Setting and $t = 2 \arccos(\beta/2)$, the relevant matrix elements of the flat band projector between the a -resonators on the zigzag edge at positions m_i and m_j (i.e., those relevant to our study) are

$$P_{ij}(\beta) = \langle a_{0m_i} | \mathbf{P} | a_{0m_j} \rangle = \frac{1}{\beta^2 \pi} \int_t^\pi dk (\beta^2 - 2 - 2 \cos k) \cos[k(m_i - m_j)]. \quad (77)$$

Setting $m = |m_i - m_j|$, the integral can be calculated exactly and for $\beta < 2$ we end up with

$$P_{ij}(\beta < 2) = \frac{t}{\beta^2 \pi} \times \begin{cases} 2 \sin(t) + (\beta^2 - 2)(\pi - t) & \text{for } m = 0 \\ (1 - \beta^2/2) \sin(t) - 2 \arccos(\beta/2) & \text{for } m = 1 \\ (2 - \beta^2)s(m) + s(m+1) + s(m-1) & \text{for } |m| \geq 2 \end{cases}, \quad (78)$$

where $s(x) = \sin(tx)/(tx)$ is a cardinal sine function with a rescaled argument, depending on t , hence on β . For $\beta \geq 2$, the lower bound of integral (77) vanishes and we obtain

$$P_{ij}(\beta \geq 2) = \begin{cases} 1 - 2/\beta^2 & \text{for } m = 0 \\ -1/\beta^2 & \text{for } m = 1 \\ 0 & \text{for } |m| \geq 2 \end{cases}. \quad (79)$$

Thus, interestingly, P_{ij} scales as the inverse of the distance m between emitters for $\beta < 2$, while it becomes strictly compact for $\beta \geq 2$.

Notice that $P_{ii}(\beta)$ corresponds to the integral in Eq. (37), for which reason the normalization constant in the effective cavity modes introduced before can be in general expressed as $\mathcal{A} = 1/[P_{ii}(\beta)]^2$. Furthermore, as it appears evident from the form of the cavity mode, we have that $c(0, m_i - m_j) = P_{ij}(\beta)$. Thus, $P_{ij}(\beta)$ also represents the shape of the effective cavity mode computed on the zigzag edge.

In the following, we leverage this knowledge in order to discuss the scaling at long distances of the cavity modes, both on the edge and toward the bulk.

VIII. SHAPE OF THE EFFECTIVE CAVITY MODES

As discussed in the main text, each qubit coupled to the edge of graphene seeds its *own* effective cavity. Although the analytic expression of such cavity is cumbersome, still one can study the shape of such cavity at long distances in order to highlight its scaling.

We start by looking at the shape of the cavity mode along the zigzag edge, namely the quantity $c(0, m)$ in the $m \rightarrow \infty$ limit. Recalling that this quantity is equivalent to the FB projector, for $m \geq 2$ this quantity can be written as

$$c(0, m) \propto (2 - \beta^2) \frac{\sin tm}{m} + \frac{\sin t(m+1)}{m+1} + \frac{\sin t(|m|-1)}{m-1}, \quad (80)$$

where $t = 2 \arccos(\beta/2)$. In the $m \rightarrow \infty$ limit, one can expand

$$\frac{1}{|m| \pm 1} = \frac{1}{|m|} \left(\frac{1}{1 \pm |m|^{-1}} \right) \simeq \frac{1}{|m|} \left[1 \mp \frac{1}{|m|} + \frac{1}{|m|^2} \right] \quad (81)$$

and so, recalling that $\sin t(m \pm 1) = \sin tm \cos t \pm \cos tm \sin t$, where a is a real constant, we get that the FB projector can be expanded as

$$c(0, m \gg 1) \propto -\beta \sqrt{4 - \beta^2} \frac{\cos(tm)}{m^2} + (\beta^2 - 2) \frac{\sin(tm)}{m^3}. \quad (82)$$

This entails that the wavefunction of the cavity mode on the edge scales as m^{-2} . Accordingly, also $P_{ij} \propto |m_i - m_j|^{-2}$.

The computation of the scaling along the bulk direction is a bit more involved. For the sake of simplicity, we start by focusing on the cavity seeded by a single qubit in the $\beta = 1$ case. The amplitude of the effective cavity [cf. (6)] on cavity a_{nm} is given by

$$c(n, m) = \frac{1}{\sqrt{2\pi}} \int_{\frac{2\pi}{3} < |k| < \pi} dk \mathcal{N}_k \varepsilon_k(n, m) = \frac{(-1)^n}{\sqrt{2\pi}} \int_{\frac{2\pi}{3} < |k| < \pi} dk [-(1 + 2 \cos k)] e^{ik(n/2+m)} \exp\left\{-\frac{n}{\lambda_k}\right\} \quad (83)$$

where $\mathcal{N}_k = \sqrt{-(1 + 2 \cos k)}$ and $\varepsilon_k(n, m)$ is the amplitude of edge mode \mathcal{E}_k on the corresponding cavity. From this expression, one can see the cavity mode as a superposition of edge modes, each with its own localization length λ_k ranging from 0 to infinity. Now, if we are interested on studying $c(n \gg 1, m)$, we could argue that only edge modes which are extremely extended i.e., those for which $\lambda_k \gg 1$, will contribute to the integral in this limit. For this reason, one can expand the integrand around $k = 2\pi/3$ and, recalling that $\exp\{-1/\lambda_k\} = 2 \cos(k/2)$, we end up with

$$c(n, m) \propto \int_{k_0}^{k_1} dk \left[\sqrt{3} \left(k - \frac{2\pi}{3} \right) - \frac{3n+1}{2} \left(k - \frac{2\pi}{3} \right)^2 \right] \cos\left(k \left(\frac{n}{2} + m \right)\right), \quad (84)$$

where $k_0 = 2\pi/3$ and $k_1 - k_0 = \frac{2\sqrt{3}}{3n+1}$ are chosen in order to guarantee that the integrand is still positive over the whole integration path (as the original integrand was). Evaluating this integral gives a number of terms depending on powers of n . The term at leading order for $n \gg 1$ scales as n^{-2} . Luckily, this argument still can be made in the general $\beta < 2$ case noticing that the integrand we get as a result of the expansion has the same form as the one discussed here.

In the end, we get that, both on the edge and along the open direction, the cavity mode wavefunction $c(n, m)$ scales as a power-law with exponent -2 .

IX. QUBIT-QUBIT INTERACTION POTENTIAL IN THE DISPERSIVE REGIME

The dispersive regime is reached when the detuning of the qubits' frequency and the FB is much bigger than the interaction strength i.e., $|\Delta| \gg \Omega$. In principle, one could go to this regime in the gapless system, but this would be detrimental as, since the decay rates into bulk scales linearly with $|\Delta|$, it would entail a strong dissipation into bulk modes. To circumvent this issue, one can open a gap in the system by setting $\delta \neq 0$, which would shift the FB frequency to δ . In this way, one can tune the qubits' frequency into the bandgap i.e., $|\Delta| < \delta$, allowing for the dispersive regime to be reached while also avoiding any leak of the qubits' population in the bulk.

Thus, assuming both $|\Delta| < \delta$ and $|\Delta - \delta| \gg \Omega$ (dispersive condition) and considering only the case in which the qubits are coupled to the edge, we can expand the interaction Hamiltonian of the full system up the second order in perturbation theory [56], yielding the effective Hamiltonian (valid provided that the bath is initially in its vacuum state) $\mathcal{H}_{\text{eff}} = \sum_{ij} \mathcal{K}_{ij} \sigma_i^\dagger \sigma_j$, where the interaction potential \mathcal{K}_{ij} reads

$$\frac{\mathcal{K}_{ij}}{g^2} = \frac{1}{\Delta - \delta} c(0, |m_i - m_j|) + G_{\text{bulk}}(\Delta), \quad (85)$$

where $c(0, m)$ is the cavity mode wavefunction (equivalent to the matrix element of the FB projector) [see section VII] and $G_{\text{bulk}}(\Delta)$ is the matrix element of the bulk modes' Green's operator, computed at the qubit frequency Δ , computed between the two resonators to which qubit i and j are coupled to.

Although being a 2D system, for which the general theory developed in Ref. [21] would predict the bulk contribution $G_{\text{bulk}}(\Delta)$ to be negligible with respect to the one coming from the FB, in this case we have to include this term in order to reproduce the correct shape of the interaction potential. This stems from the fact that, under the considered choice of BCs, the system is mapped into a collection of 1D systems, entailing in particular the divergence of the density of states of bulk modes at the edge of each bands in the $\delta \neq 0$ case. This addition of this term might prejudice the scaling of the interaction potential but, hopefully, this is not the case, as we show next.

The bulk modes' Green's function entering in the interaction potential reads

$$G_{\text{bulk}}(\Delta) = \sum_{\mu=\pm} \int_{-\pi}^{\pi} dk \int_0^{\pi} dq \frac{\langle a_{0m_i} | \mathcal{B}_{\mu}(k, q) \rangle \langle \mathcal{B}_{\mu}(k, q) | a_{0m_j} \rangle}{\Delta - \omega_{\mu}(k, q)}, \quad (86)$$

which in the $\beta = 1$ (pristine/isotropic graphene) case can be simplified as

$$G_{ij}(\Delta) = \frac{2(\Delta + \delta)}{\pi^2} \int_0^{\pi} dk \int_0^{\pi} dq \frac{4 \cos^2(k/2) \sin^2(q) \cos(k|m|)}{[\omega^2(k, q) - (\delta/J)^2][\Delta^2 - J^2 \omega^2(k, q)]}. \quad (87)$$

We now expand $[\Delta^2 - J^2 \omega^2(k, q)]^{-1}$ around its minimum as

$$\frac{1}{\Delta^2 - J^2 \omega^2(k, q)} \simeq \frac{1}{\Delta^2 - \delta^2} \left[1 + \frac{3(k - 2\pi/3)^2/2 + (q - \pi)^2/2}{\Delta^2 - \delta^2} \right] \quad (88)$$

which, upon substitution yields

$$\begin{aligned} G_{\text{bulk}}(\Delta) &\simeq \frac{1}{\Delta - \delta} \frac{1}{\pi^2} \int_0^{\pi} dk 8 \cos^2(k/2) \cos(k|m|) \left(1 + \frac{3(k - 2\pi/3)^2}{2(\Delta^2 - \delta^2)} \right) \left(\int_0^{\pi} dq \frac{\sin^2 q}{\omega^2(k, q) - (\delta/J)^2} \right) \\ &+ \frac{1}{2(\Delta - \delta)(\Delta^2 - \delta^2)} \frac{1}{\pi^2} \int_0^{\pi} dk 8 \cos^2(k/2) \cos(k|m|) \left(\int_0^{\pi} dq \frac{(q - \pi)^2 \sin^2 q}{\omega^2(k, q) - (\delta/J)^2} \right). \end{aligned} \quad (89)$$

The first integral in square brackets (first row) can be evaluated exactly, yielding

$$\int_0^{\pi} dq \frac{\sin^2 q}{\omega^2(k, q) - (\delta/J)^2} = \frac{\pi}{8 \cos^2(k/2)} [4 \cos^2(k/2) - 1] = \frac{\pi}{8 \cos^2(k/2)} [1 + 2 \cos k], \quad (90)$$

while the second one is computed numerically yielding an almost constant value of $\simeq 4$ for every value of k , meaning that

$$\begin{aligned} G_{ij}(\Delta) &\simeq \frac{1}{\Delta - \delta} \left(1 + \frac{2}{\Delta^2 - \delta^2} \right) \frac{1}{\pi} \int_0^{\pi} dk [1 + 2 \cos k] \cos(k|m|) \\ &+ \frac{3}{(\Delta - \delta)(\Delta^2 - \delta^2)} \frac{1}{\pi} \int_0^{\pi} dk 4 \cos^2(k/2) (k - 2\pi/3)^2 \cos(k|m|). \end{aligned} \quad (91)$$

Now the first integral gives a contribution that is exactly zero for $|m| > 2$ and so we can drop it if we are interested in the long-distance scaling of this term. The second integral can be rewritten as

$$\begin{aligned} \frac{1}{\pi} \int_0^{\pi} dk 4 \cos^2(k/2) (k - 2\pi/3)^2 \cos(k|m|) &= \frac{2}{\pi} \int_0^{\pi} dk [1 + \cos k] (k - 2\pi/3)^2 \cos(k|m|) \\ &= \frac{2}{\pi} \int_0^{\pi} dk (k - 2\pi/3)^2 \cos(k|m|) + \frac{1}{\pi} \int_0^{\pi} dk [\cos k(|m| + 1) + \cos k(|m| - 1)] (k - 2\pi/3)^2 \end{aligned} \quad (92)$$

which can be evaluated analytically, giving a rather involved expression. Luckily, one can show that in the $|m| \rightarrow \infty$ limit, this expression yields a contribution scaling as $|m|^{-2}$. Knowing that, it is clear that both contributions to the interaction potential \mathcal{K}_{ij} will have the same scaling for long distances, the same as the cavity mode. As a result, one gets power-law mediated interactions with an exponent equal to -2 .

X. EXPERIMENTAL IMPLEMENTATION

The system presented in the main text can be directly implemented using superconducting lumped-element LC resonators [41, 42, 44] arranged in a honeycomb lattice [see Fig. S1(a)]. Each lattice site consists of a parallel combination of inductor L_g and capacitor C_g connected to ground. Neighboring sites are coupled via capacitors C_c , creating the nearest-neighbor hopping required for the tight-binding model. The resonator frequency is determined by $\omega_r = 1/\sqrt{L_g C_\Sigma}$, where $C_\Sigma = C_g + zC_c$ represents the total capacitance at each site and z is the coordination number. For sites with different coordination numbers (such as edge sites), the ground capacitance is adjusted to maintain a fixed C_Σ , thus ensuring uniform on-site frequencies across the lattice. In the tight-binding limit where $C_c \ll C_\Sigma$, the hopping amplitude between neighboring sites takes the simple form $J = (C_c/C_\Sigma)\omega_r/2$. This capacitive coupling scheme works particularly well with compact, high-impedance resonators that have been implemented in circuit QED setups [35, 44]. While we focus on capacitive coupling, inductive coupling provides an alternative implementation route with similar physics [57, 58].

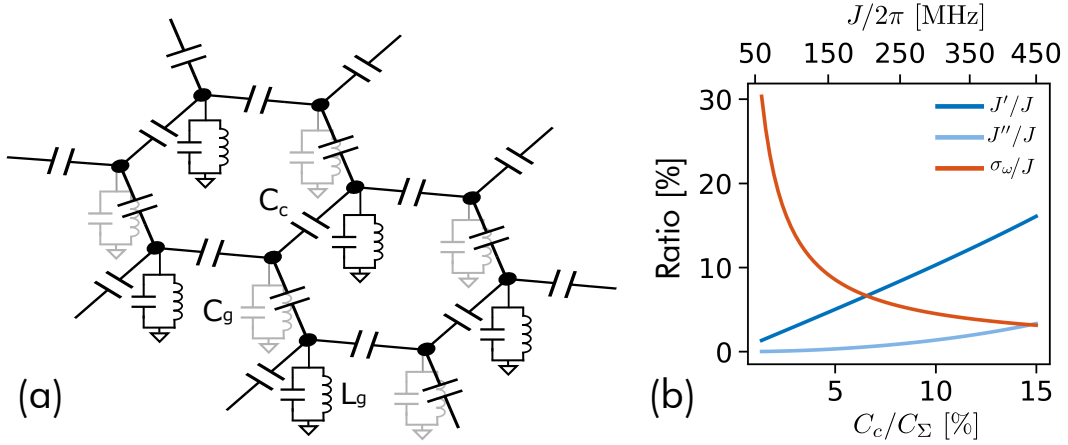


Figure S1. (a) Electrical circuit schematic of hexagonal lattice. Each site contains an LC resonator (L_g, C_g) with neighboring sites coupled via capacitors C_c . (b) Scaling of nearest-neighbor hopping J , second-nearest-neighbor hopping J' , third-nearest-neighbor hopping J'' , and frequency disorder σ_ω with coupling strength C_c/C_Σ . Stronger coupling enhances both the desired nearest-neighbor hopping J and parasitic longer-range hoppings (J', J'') while reducing relative disorder effects.

The edge termination is naturally implemented in finite-size devices. Interestingly, since edge modes appear only for specific edge shapes—such as zigzag or bearded edges—and are absent in others, like the so-called armchair configuration [15], we expect the coherent dynamics described in the main text to be observable or not depending on the specific choice of edge shape. One practical approach to explore these two different scenarios employs a rectangular geometry with two zigzag edges that host the flat band edge modes, while the other boundaries form armchair edges that do not support edge states. This represents just one possible implementation; other geometries that incorporate zigzag edges would equally support the desired edge mode physics. As an additional experimental verification, qubits placed along the trivial (armchair) edges can serve as control measurements, demonstrating that the predicted qubit-edge mode coupling and resulting dynamics occur only in the presence of the topological flat band edge modes.

To accurately model the system beyond the tight-binding approximation, we employ a full circuit analysis using Lagrangian formalism [44, 59]. The system is described by constructing the complete capacitance matrix \mathbf{C} , which includes both the self-capacitance C_Σ of each resonator and the coupling capacitance C_c between nearest neighbors. Combined with the inverse inductance matrix \mathbf{L}^{-1} (diagonal with elements $1/L_g$), this yields the system Hamiltonian $\mathbf{H} = \sqrt{\mathbf{L}^{-1}\mathbf{C}^{-1}}$, whose eigenvalues correspond to the collective mode frequencies.

Two primary non-idealities affect the experimental realization: *long-range* hopping terms and *disorder* in the system's parameters. Mathematically speaking, long-range hopping terms are a byproduct of the inversion of the capacitance matrix \mathbf{C} . This means that, even when we physically implement only nearest-neighbor capacitive couplings C_c , the circuit equations generate second-nearest-neighbor hoppings J' , third-nearest-neighbor hoppings J'' , and higher-order terms. These arise from the collective nature of the electromagnetic modes and represent an important deviation from the ideal tight-binding model. These long-range hopping terms are further enhanced by spurious capacitances between non-adjacent sites, which arise from electric field coupling in any physical implementation. At the same time, fabrication variations in both inductance and capacitance values lead to disorder in circuit parameters. Importantly, while disorder in both on-site frequencies and hopping amplitudes is present, only the on-site frequency disorder (diagonal disorder) breaks the chiral symmetry of the system. Disorder in hopping amplitudes preserves chiral symmetry and thus does not affect the frequency of the edge modes discussed in the main text [60]. Therefore, we focus our analysis on the on-site frequency disorder with standard deviation σ_ω arising from variations in L_g and C_g .

In both cases, chiral-symmetry breaking gives the zero-energy flat band a finite spectral width and causes the edge modes, which ideally reside only on the a -sublattice, to acquire non-zero amplitude on both sublattices. Preliminary analysis shows that, in order to observe the presented phenomenology, we need to work in a parameter region where this spectral width is small compared to the qubit coupling $g/2\pi$. Moreover, for sufficiently large disorder compared to the hopping strength, the system enters an Anderson localization regime [61] where all modes become spatially localized at random positions.

In light of the above, the choice of circuit parameters involves a fundamental trade-off [see Fig. S1(b)]. For fixed resonator frequency, increasing the coupling strength by raising the ratio C_c/C_Σ improves robustness against disorder by increasing all hopping strengths (J , J' , J'') but maintaining fixed frequency disorder. However, stronger coupling simultaneously enhances the unwanted higher-order hopping terms, making the nearest-neighbor approximation in the main text less accurate.

Through numerical simulations of the full circuit Hamiltonian, we find that the parameters mentioned in the main text – i.e., $\omega_r/2\pi = 6$ GHz, $J/2\pi = 100$ -200 MHz and $g/2\pi = 20$ MHz – represent a reasonable compromise (see Fig. S1). For these values, the next-nearest-neighbor hopping J'/J and frequency disorder σ_ω/J are in the range 5 – 10 % with the spectral width of the flat band being reasonably smaller than $g/2\pi$. Although those non-idealities are significant, preliminary analysis suggests that the predicted effects should remain observable.